UCLouvain

École polytechnique de Louvain

Coupling 1D river and 2D floodplain for modelling fluvial inundations

Author: **Arthur Golenvaux**
Supervisors: **Emmanuel Hanert, Jonathan Lambrechts**
Readers: **Sandra Soares Frazao, Insaf Draoui**
Academic year 2022–2023
Master [120] in Mechanical Engineering

Abstract

With the escalating impact of river floods attributed to global warming, it has become imperative to adapt our lands accordingly. The construction of retention areas and the preservation of floodplains offer promising solutions in this regard, necessitating the use of numerical modeling to understand the dynamics of river flooding. In this thesis, we introduce a discontinuous Galerkin explicit method that effectively couples a 1D river model with a 2D floodplain representation. The exchange of mass is facilitated through the weir equation, employing lateral coupling between linear 1D elements and triangular 2D elements that accurately handle wetting-drying fronts. To validate the model, we conduct laboratory-like test cases, comparing the results with those obtained from a fully constructed 2D model. Furthermore, we perform a more realistic test on a bifurcation, which convincingly assesses the peak flow in the river. Notably, our model offers a significant time advantage while delivering satisfactory results in the study of river floods.

Remerciements

Je tiens à exprimer ma profonde gratitude envers l'équipe encadrante de SLIM. Leur patience et bienveillance tout au long de mon séjour en Erasmus, et jusqu'à la fin de l'année, ont été d'une aide précieuse. Tout d'abord, je souhaite remercier Emmanuel Hanert pour ses enseignements précieux, son implication et sa disponibilité constante tout au long de ce mémoire. Je tiens également à remercier Jonathan Lambrechts pour son aide avec le code, ses idées et ses remarques toujours constructives qui m'ont permis de mieux identifier les objectifs à atteindre. Je souhaite également remercier Lauranne et Riana pour leur assistance à plusieurs reprises, notamment pour la rédaction, ainsi que Miguel pour son aide précieuse dans l'implémentation du code et ses débogages incroyablement efficaces. Enfin, je tiens tout particulièrement à remercier Insaf pour son soutien inestimable tout au long de l'année, même à distance, sa patience et sa disponibilité. Sans elle, ce mémoire n'aurait pas été possible.

J'aimerais également exprimer ma gratitude envers ma famille et les membres de l'Orchestrakot pour leur soutien. Je tiens également à remercier Simon, Charlotte, Juliette, Antoine (x2), Arthur pour leur entraide et leurs conseils précieux, ainsi qu'Elise pour son écoute, sa patience et ses précieux conseils.

Disclaimer:

The contents of this document were generated with the assistance of Chat GPT. However, it is important to note that Chat GPT was solely used as a writing aid for tasks such as grammar and style correction, and at no point was it used to generate substantive content. The ideas and concepts presented in this report are entirely the author's own and have not been influenced by Chat GPT.

Contents

Chapter 1

Introduction

1.1 The growing problem of river flooding

Over time, river flooding has been one of the most destructive natural disasters, causing significant harm to society. Although it may not be the most deadly natural catastrophe, it certainly affects the largest number of people on earth and occurs more frequently than any other. According to data from a 1998 and 2017 report by UNISDR and the CRED, floods accounted for 43.4% of natural disasters worldwide and affected 2 billion people [1]. In European Union and the United Kingdom, the damage caused by river flooding is estimated at 7.8 €billion per year, while more than 170,000 people are exposed to these events annually [2].

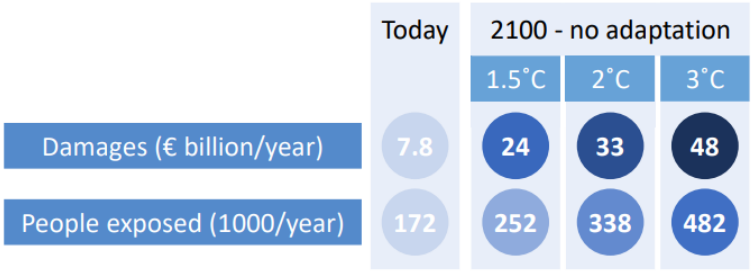

Figure 1.1: Annual damages and the population at risk from river flooding in the EU and UK in 2020 ("Today") and projected for 2100 under 3 global warming scenarios. "No adaptation" refers to present-day flood protection measures.

The situation is becoming even more dire due to urbanization and an increase in greenhouse gas emissions, which have all contributed to a rise in the frequency and intensity of heavy precipitation events [3]. As a result, the probability of flood occurrences has also increased [4]. In the case where no adaptation measures are

taken, a report from the Joint Research Centre (JRC) estimates that the economic loss in the European Union will reach nearly 50 €billion/year by 2100 with global warming of 3°C [2] (Fig. 1.1).

In addition to the direct human and material costs of these events, floods pose also long-term effects resulting from the transmission of viral diseases, especially water-borne infections [5]. Developing countries are particularly vulnerable to the adverse health consequences of floods due to limited public-health infrastructure and inadequate emergency response capabilities. With the global population, urbanization, temperature continuing to rise, and the risk of pandemics on the horizon, it has become necessary to find effective solutions to prevent and mitigate the impact of flooding. The restoration and the conservation of floodplains, low-lying areas adjacent to rivers enabling the river water to spread over its surroundings, seems to be the solution to follow as we will see in the next section.

1.2 Usage and utility of floodplains during flooding

1.2.1 The solution for river flooding in EU

A JRC technical report [2] investigates four solutions to alleviate the problems of river flooding in Europe :

- Strengthening of dyke systems,
- Damage reduction measures for buildings,
- Relocation to the flood-safe area,
- Development of retention areas to store flood waters.

The economic and social contribution of the different solutions according to the climate change scenario is shown in Fig. (1.2). We can observe that the relocation solution does not significantly reduce either the annual damages or the exposed population, while strengthening the dikes brings an almost three-fold reduction in these factors. But dyke systems have several social and environmental drawbacks. Heightening river dykes can increase the magnitude of peak flows downstream, thus amplifying flood hazard and risk downstream. The solution that yields the greatest reductions has proven to be the building of retention area, which could provide a reduction from 64% to 82% in economic damage and population exposure albeit with a high benefit-to-cost ratio [2]. Retention area function as floodplains during a flood, where the excessive volume of water fills these areas, thus reducing the peak

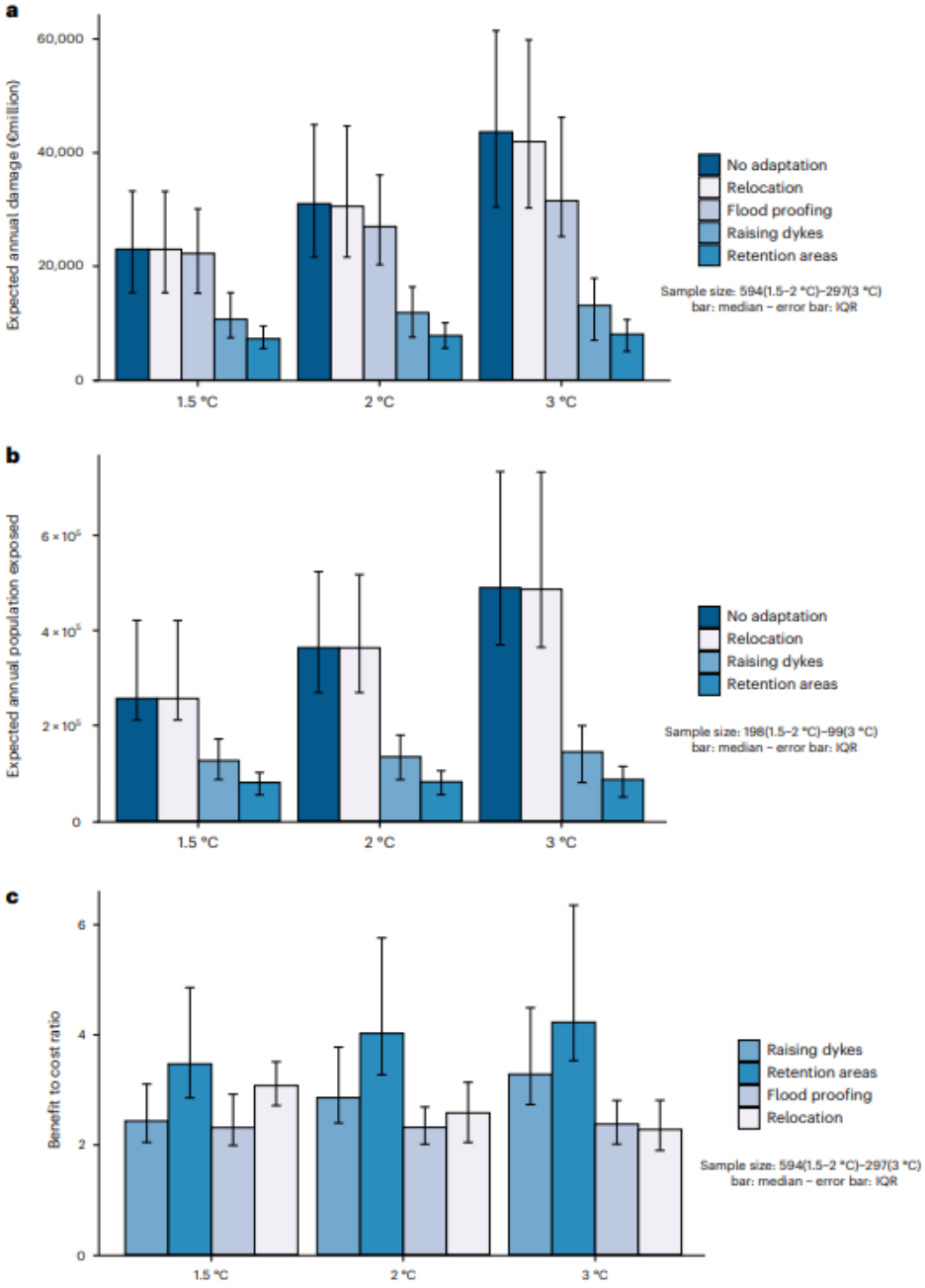

Figure 1.2: Outcomes for the four adaptation strategies considered under 1.5, 2 and 3 °C. a) future undiscounted economic damage and b) population exposed for the year 2100. c) the benefit-to-cost ratio calculated from total discounted benefits and costs over the period 2020-2100.

flow in the river. Mentaschi et al.[6] further suggest that the problem of retention area which would no longer be available for some land uses is exposed, and they estimate that the overall floodplains area required would be less than 2% of the overall cropland area in Europe. In another article, Wing O.E.J. Bates P.D. et al. [7] mention that in the United States, "*Strategic conservation of floodplains would avoid unnecessarily increasing the economic and human costs of flooding while simultaneously providing multiple ecosystem services*". Through these two examples, we understand the importance of these low-lying areas and the interest that we can have in studying their behavior. Whether it is a retention area or a floodplain, through this thesis we will study the dynamic of water spreading over these lands coming from a flooded river, which is essential to configure and use properly these areas.

1.2.2 Floodplains

But what are exactly floodplains? The Cambridge Academic Content Dictionary gives the definition "*an area of low, flat land near a river that often floods when the level of the river rises and flows over its sides*". These lands are generally very fertile due to the sediments that are deposited during floods and therefore have greatly varied topology, composition, etc. depending on environmental and geographic parameters. While floodplains play a critical role in agriculture, erosion control, biodiversity, and water quality, their function as "natural sponges" during periods of flooding is particularly noteworthy. As floodwaters spread onto floodplains, a portion of the volume is absorbed and stored in the soil, replenishing groundwater supplies. An important feature of some floodplains, on which we will focus in this thesis, is the presence of levees along the longitudinal boundary of the river. Natural levees are formed by the deposition of suspended sediments along the floodplain edge which are supplied from the main channel during overbank flow. The formation of levees is composed of three steps (Fig.1.3, [8]) :

1. Sediment particles are lifted into the water column when the turbulent motion exceeds the submerged particle weight ;
2. The particles are transported laterally toward the floodplain ;
3. The lift force no longer exerts itself outside the river and the sediments are therefore deposited on the border.

Hydraulic conditions define the time available for settling and thus how far the suspended sediments can be transported onto the floodplain before they will be deposited. This explains why the levees are smaller in tidal rivers compared to inland rivers.

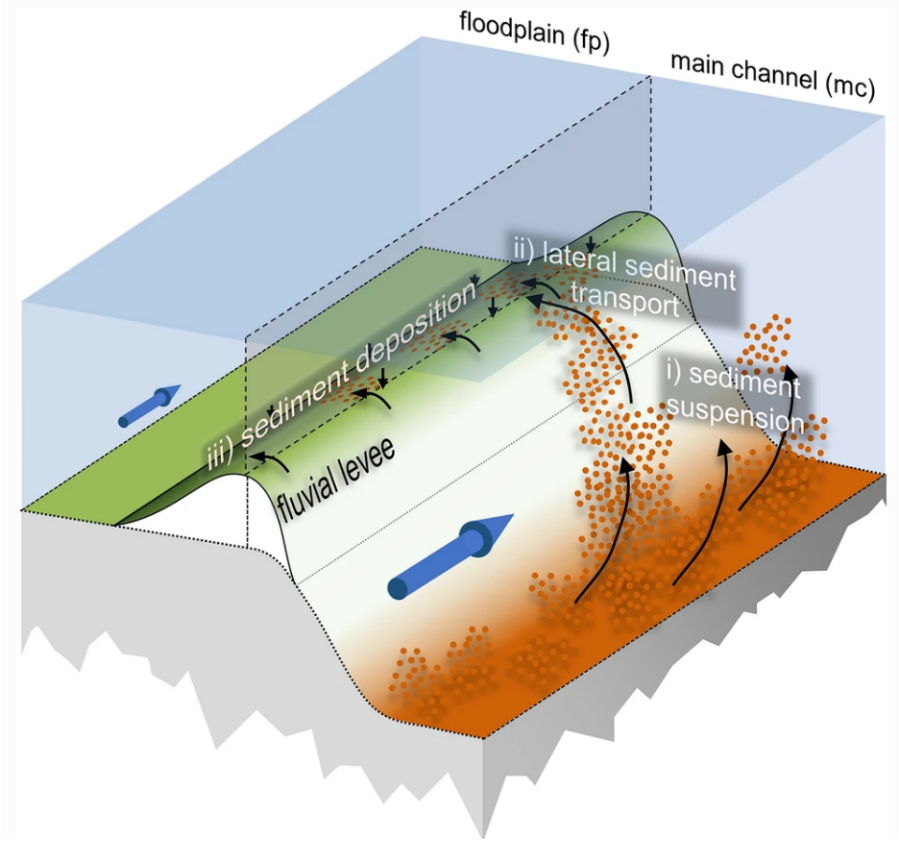

Figure 1.3: Scheme of the formation of levee (from [8]).

The modeling and characterization of floodplains is a complex task due to their variety, complex transient functioning, and their specific topography. It is therefore crucial to take into account all these parameters when studying the effect of floodplains. Here we will use numerical models to study their functioning.

1.3 River flood inundation modeling

As discussed in the previous section, floodplains are intricate areas with specific topography, and studying their behavior during floods has become increasingly important. Numerical methods offer several advantages over experimental methods, such as predictive capabilities, cost-effectiveness, and reproducibility. These methods can be easily replicated and modified, making them highly advantageous. However, empirical methods are still very useful when combined with other techniques to gain a comprehensive understanding of the behavior of rivers and other

natural systems. In many studies, empirical methods are primarily used for flood monitoring and for validating data obtained from other methods [9].

1.3.1 Numerical methods to model flows

For almost 80 years, numerical methods allow us to approach the solution of nonlinear partial differential equations that were not analytically solvable in fluid dynamics [10]. When modeling complex structures and detailed flow dynamics, numerical models are necessary. However, there are many different numerical methods to choose from, and selecting the most appropriate one for a given modeling task depends on various factors, such as the desired output, available data, and computational resources. The trade-off between time and precision is crucial, and the choice between 1D, 2D, or 3D numerical models is essential depending on the desired study.

Rivers, in which the dominant flow directions and forces follow the general river flow path, are thus usually modeled sufficiently with 1D models. The 2D models are necessary when the flow is not uni-directional, as in the floodplain or as the river mouth, while 3D models are uncommon in the context of modeling river flooding because the accuracy gained by such a complex model is not important enough compared to the additional time required to compute it. 3D models are mainly used for specific phenomena occurring in the flow, such as turbulence, sediment transport, or in the estuary when there is stratification [11]. Since the focus of this thesis is on the hydrology of flood inundation and not on sediment transport or other specific details, we will not be discussing the implementation and use of 3D models any further.

To model river flood spreading on a floodplain, 2D models appear to be the best solution since they can represent the lateral dynamic on the surface area. When modeling wetting-drying processes in floodplains, instabilities can occur at the wet/dry front, and the rapid transition of wet/dry interfaces and mass conservation may not always be ensured. In consequence, a wetting and drying algorithm that can be activated when this phenomenon occurs and ensure stability and accuracy is necessary, and the one used in this thesis will be described later.

While it is essential to model the floodplain using a 2D algorithm, modeling the course of the river in 2D is not necessary, and we could increase speed by modeling it in 1D. Therefore, a solution is to couple a river modeled in 1D with the floodplain calculated in 2D. This thesis will describe and explain the modeling of the communication between the two models, specifically how information will be exchanged between these two environments.

1.4 Coupling 1D and 2D models

Regarding the 1D-2D coupling methods in the literature, the main discussion typically revolves around the interaction between the models. Specifically, whether this interaction is solely through mass transfer or if it also includes momentum transfer. In this section, we will present different coupling methods that employ various strategies and discuss their strengths and drawbacks. This presentation of the models will later allow us to position our method within the existing literature while justifying certain choices based on previously obtained results.

Brufaua et al. [12] describe an explicit finite volume method where for each time step, the 1D and 2D models are first computed separately, then corrected using "coupling zone" where the total mass and the momentum are conserved (Fig 1.4). Two structures of coupling are described, the lateral and the frontal coupling.

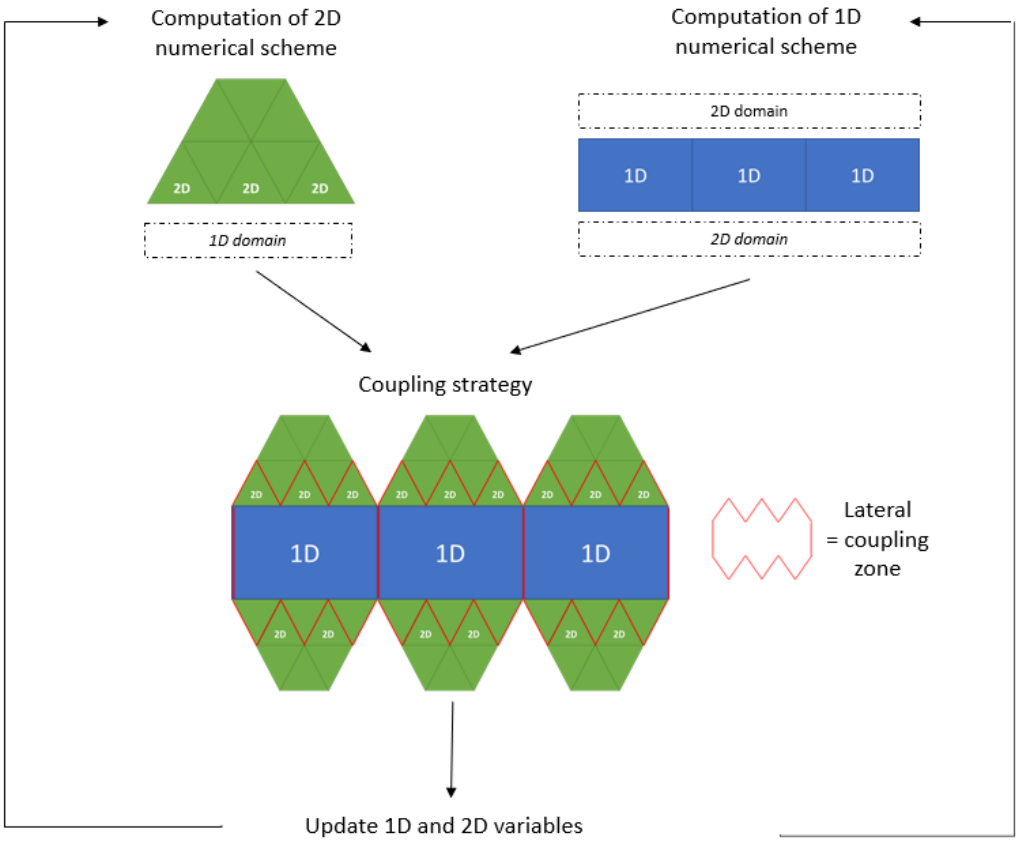

Figure 1.4: Flowchart of first coupled scheme ([12]).

Frontal coupling means that the 2D area cuts and interrupts the 1D channel transversely instead of lateral coupling where the channel is not crossed by the 2D zone, this one extending along both sides of the river (Fig 1.5). They specify that the

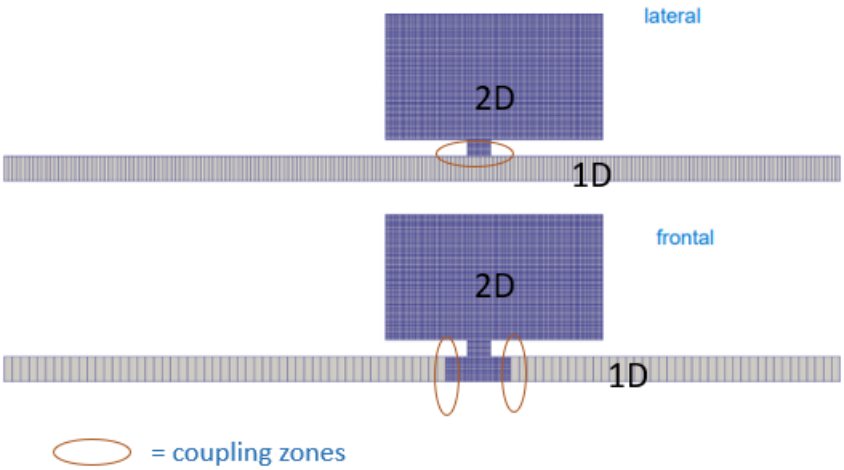

Figure 1.5: Frontal and lateral coupling with their coupling zones.

imposition of momentum transfer should only occur in the case of supercritical flow, while Only Mass Conservation (OMC) condition is imposed when the flow between the models is subcritical. The model is then used in a laboratory test case, where a levee is breaking in a channel containing a small floodplain, and in a real case scenario, the Tiber River. The flooded area of the model is compared with the one of a reference full 2D model, and it appears that even if frontal coupling gives slightly more accurate results, lateral coupling is more relevant in the case of real-world river flow modeling since the border between the 1D and 2D regions is more easily defined.

Fernández-Nieto et al.[13] present a method using finite volume schemes where a local 2D model (representing the retention area) is superposed over a 1D main channel model with non-flat topography using the shallow-water equations. The information between the models is made through a coupling source term acting on the conservation of mass and momentum. Numerical test cases show the efficiency and robustness of the discretization done and show that the superposing approach is relevant.

Kuiry et al. [14] propose a method where a 1D finite volume river spread excess flood water onto an unstructured triangular grid forming the floodplain (Fig 1.6). The interaction between the channel and the floodplains is made only by mass

transfer and the model ignores the velocities on the floodplain. Yet, the model was

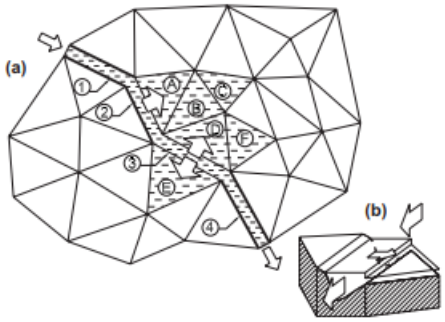

Figure 1.6: Scheme of the coupling system presented in [14].

used for a hypothetical flood scenario and also applied to the river Severn, predicting the inundation extents for naturally occurring floods with sufficient precision.

Bladé et al. [15] couple a 1D river laterally connected to the 2D floodplain through a source term describing the weir equation, in a finite volume scheme once again. As previously explained, inland rivers are generally composed of levees, and this model takes into account this geometrical particularity and compares them to work as a flow over a river embankment or protection dikes (Fig. 1.7). The mass exchange between the floodplain and the river is thus conserved through this weir equation describing the discharge, going from the floodplain to the main river or the opposite. This method is the starting point of the method that will be used in this thesis.

We have seen a glimpse of the variety of methods that can be applied to couple 1D and 2D models, and we have observed that momentum transfer is not always necessary when comparing the model with a reference, whether it is a full 2D model or field data. The difference lies primarily in the objective of the method. If the aim is to demonstrate the extent of a flooded area, then mass conservation appears to be sufficient. However, if the goal is to analyze more complex dynamic phenomena, such as meander shortcuts, it is preferable to use a method that transfers momentum. One of the main differences with the methods presented here is that we will not be using a finite volume method, but rather a Discontinuous Galerkin explicit method. The scheme used will be presented later in this thesis.

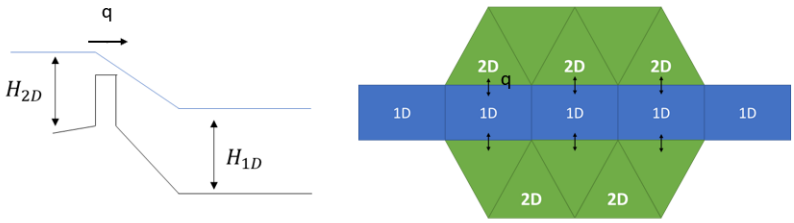

Figure 1.7: Scheme of the coupling system presented in [15], H_{1D} and H_{2D} respectively the height of water in the 2D floodplain and in the 1D river, with q the discharge.

1.5 Presentation of the thesis

We will begin by discussing the methods used to model river flooding, starting with an overview of the SLIM model. SLIM is a multi-scale model of the land-sea continuum designed to simulate water and tracers dynamics in a variety of environments, including rivers, floodplains, and estuaries. We will focus specifically on the computation of the SLIM1D module, which is used to model flows in branching river networks, as well as the SLIM2D module, which includes a Wetting and Drying Algorithm to model the floodplain inundation.

Next, we will present the 1D-2D coupling method and the algorithm that we implemented to model river flood spreading on a floodplain. This will include a description of the equations and hypotheses used in the algorithm.

We will then present laboratory-like tests made to ensure the mass conservation on the coupled model is correct and to compare the mass and energy variation between the coupled model and a full 2D reference model. A first discussion will be conducted on the obtained results.

Therefore, we will compare our model with a 2D reference model in a more realistic scenario, the case of a bifurcation. We will discuss the assumptions and limitations of the model, as well as the results obtained from our simulations.

Finally, we will conclude with a discussion of the implications of our results and how they could be used to improve our understanding of river flooding. We

will also explore potential avenues for future research, including improving the accuracy and efficiency of the 1D-2D coupling algorithm and investigating other applications of the SLIM model in the field of water resources engineering.

Chapter 2

Material and Methods

2.1 SLIM

SLIM is a hydrodynamic unstructured-mesh model which relies on the Discontinuous Galerkin finite element method. Developed at the Université Catholique de Louvain (Belgium) for over a decade, SLIM has been applied to various geographical locations worldwide to study hydrological and ecological phenomena. Among the various modules of SLIM, we focus on SLIM1D and SLIM2D models which are used in this thesis.

2.2 SLIM2D

By integrating the Navier-Stokes equations under the assumption of hydrostatic pressure and constant fluid density, one can obtain the so-called shallow-water equations (SWE). These equations provide a good representation of water flows when the water column is well-mixed and the vertical dimension is much smaller than the typical horizontal scale, making them fully suitable for modeling floodplains. The variables defining the geometry are η and h, respectively the free surface elevation and the reference depth of the domain, or the bathymetry, defined on a 0-level plane. $H = h + \eta$ is the height of the water column (Fig 2.1). The resulting conservative shallow water equations used in our model are:

$$\frac{\partial H}{\partial t} + \nabla \cdot (H\mathbf{u}) = 0 \tag{2.1}$$

$$\frac{\partial (H\mathbf{u})}{\partial t} + \underbrace{\nabla_h \cdot \frac{H\mathbf{u}H\mathbf{u}}{H}}_{1} = \underbrace{gH\nabla\eta}_{2} - \underbrace{n^2 g \frac{|Hu|Hu}{H^{\frac{7}{3}}}}_{3} + \underbrace{\nabla_h \cdot (\kappa H\ \nabla_h \mathbf{u})}_{4} \tag{2.2}$$

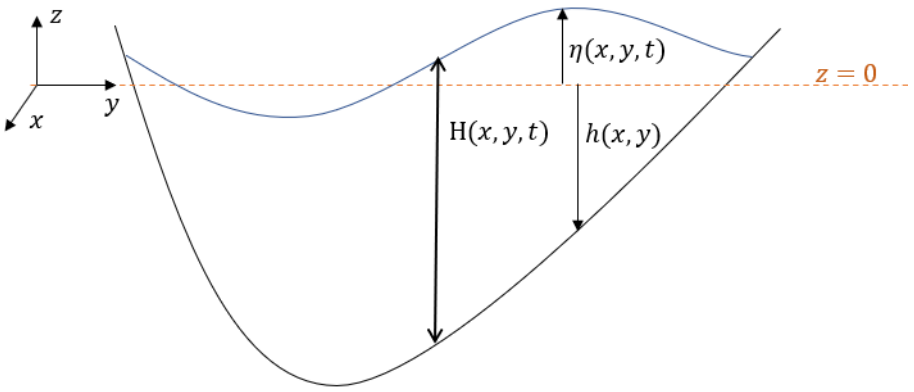

Figure 2.1: Geometry of the slim2D model.

The conservation of mass for incompressible flows is represented by Equation (1), where **u**=(u,v) is the velocity vector. Equation (2) represents the conservation of momentum, with the different terms in the equation:

1. Advection term,
2. Surface elevation gradient driving gravity waves,
3. Bottom drag term where n is the Manning-Strickler coefficient ($\frac{s}{m^{1/3}}$),
4. Turbulent momentum diffusion viscosity term,

These equations are discretized using a discontinuous Galerkin method, where the domain is divided into N triangular elements Ω_e, and then integrated and multiplied with a linear shape function ϕ_i. The vector of solution $U = (H, Hu, Hv)^T$ will be approximated with $U_{e,i}$ the nodal values of the solution :

$$U|_{\Omega_e} \simeq U_h|_{\Omega_e} = \sum_{i=1}^{3} \phi_i U_{e,i}, \tag{2.3}$$

Implicit and explicit schemes are available to solve these equations.
While the 2D model is efficient in most cases, it has limitations when the water height reaches 0, resulting in an inaccurate representation of the physical situation. This can lead to negative depth and ill-conditioned computation of velocity. To address this issue, a Wetting and Drying Algorithm is needed, which will be presented in the following section.

2.2.1 Wetting and Drying Algorithm

Water height H appears in various denominator terms in the 2D momentum conservation equations (Eq. 2.2), leading to issues when a node becomes dry and this water height approaches zero. In such cases, the associated parameters tend to infinity, resulting in unphysical outcomes. To tackle this problem, we introduce limiting values for H, replacing problematic denominators when the water height is smaller than these limits.

For the advection term (1), the limiting parameter is the hydrometric water height limit H_{lim_h} :

$$\nabla_h \cdot \frac{H\mathbf{u}H\mathbf{u}}{max(H, H_{lim_h})} \tag{2.4}$$

For Manning's bottom drag, we use two limiting values, H_{lim_d} for the dissipation and again H_{lim_h} :

$$n^2 g \frac{|Hu|}{max(H, H_{lim_h})} \times \frac{Hu}{max(H, H_{lim_d})^{\frac{4}{3}}} \tag{2.5}$$

For the viscosity term, we use H_{lim_v} as :

$$\nabla_h \cdot (\kappa H \nabla_h \frac{Hu}{max(H, H_{lim_v})}) \tag{2.6}$$

These limiting values are set to $H_{lim_v} = H_{lim_d} = 0.01m$ and $H_{lim_d} = 0.5m$.
Another algorithm has been implemented in SLIM to address additional aspects of the Wetting and Drying phenomenon and can be found in appendix A. of the report.

2.3 SLIM1D

When the horizontal flow is mainly unidirectional such as for a well-mixed river, the shallow water equations can be averaged over the width of the river leading to the 1D section-averaged shallow-water equations. SLIM1D consists of linear river segments where variable river width and depth are taken into account. The geometry of the model is described in figure 2.2. At each node in the x direction, $\eta(x,t)$ represents the mean free surface level and $b(x,z)$ the width of the cross-section for a vertical level z. $h(x)$ is the bed level. With those values, we can build the averaged section of the river $A(x,t)$ which is used for the equation of the mass in the domain as :

$$\frac{\partial A}{\partial t} + \frac{\partial Q}{\partial x} = 0 \tag{2.7}$$

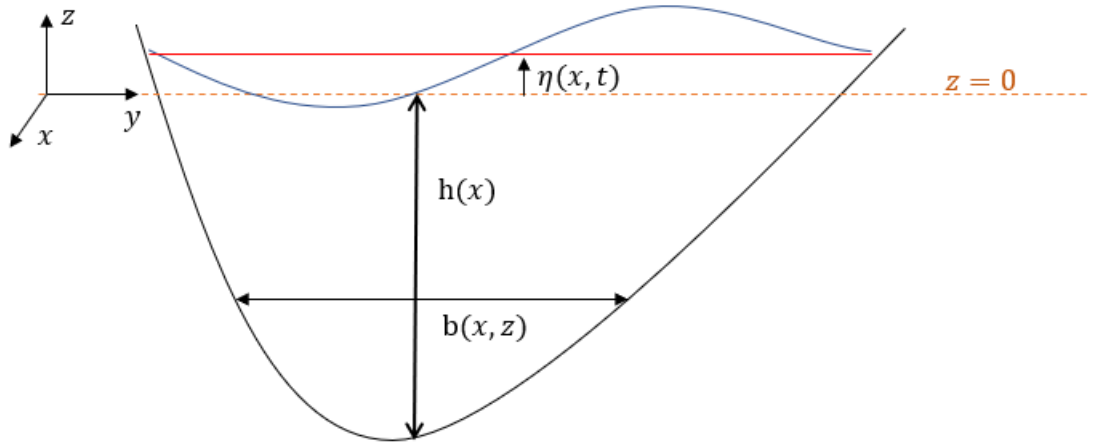

Figure 2.2: Geometry of the SLIM1D model. The blue line is the water height using the 2D model. The red line represents the mean free surface level $\eta(x,t)$.

where $Q(x,t)$ is the volumetric mean discharge. For the conservation of the momentum :

$$\frac{\partial Q}{\partial t} + \frac{\partial}{\partial x}(\frac{Q^2}{A} + \frac{P}{\rho}) = gA\frac{\partial h}{\partial x} - gQ + \frac{F}{\rho} \tag{2.8}$$

where :

- $P = \rho g \int_0^H (H-z)bdz$ is the hydrostatic pressure force exerted on the edge of the control volume,
- $\frac{\partial h}{\partial x}$ is the bed slope,
- $S = n^2 \frac{|Q|Q}{AR_h^{\frac{4}{3}}}$ is the friction-induced head loss per unit distance with n the Manning coefficient and the hydraulic radius R_h defined as the area of the flow section divided by the wetted perimeter,
- $F = \rho g \int_0^H (H-z)\frac{\partial b}{\partial x}dz$ is the along-flow component of the pressure resulting from the longitudinal width variation.

These equations are also discretized using a discontinuous Galerkin method, where the domain is divided into N linear elements.

2.4 Conservation equation form

Both 1D and 2D SWE described here are conservation equations and they can take another form :

$$\frac{\partial \mathbf{U}}{\partial t} + \nabla \cdot \mathbf{F}(\mathbf{U}) = \mathbf{S}(\mathbf{U}) \tag{2.9}$$

where $\mathbf{U}$ is the vector of unknown, $\mathbf{F(U)}$ is the flux of the conserved variables and $\mathbf{S(U)}$ is the source term.
For the 1D equation, we have :

$$\mathbf{U} = \begin{pmatrix} A \\ Q \end{pmatrix} \quad , \quad \mathbf{F(U)} = \begin{pmatrix} Q \\ \frac{Q^2}{A} + \frac{P}{\rho} \end{pmatrix} \quad \text{and} \quad \mathbf{S(U)} = \begin{pmatrix} 0 \\ gA\frac{\partial h}{\partial x} - gQ + \frac{F}{\rho} \end{pmatrix} \tag{2.10}$$

and for the 2D model :

$$\mathbf{U} = \begin{pmatrix} H \\ Hu \end{pmatrix}, \quad \mathbf{F(U)} = \begin{pmatrix} Hu \\ Huu - \kappa H \ \nabla_h \mathbf{u} \end{pmatrix}, \quad \mathbf{S(U)} = \begin{pmatrix} 0 \\ gH\nabla\eta - \gamma Hu|u| \end{pmatrix} \tag{2.11}$$

Where γHu is the drag formula, using the Manning-Strickler formula :

$$\gamma = \frac{gn^2}{H^{4/3}} \tag{2.12}$$

2.5 Manning coefficient

The parameterization of the dimensionless Manning coefficient, used in the Manning formula in the 1D and 2D equations of SLIM to represent bottom drag or bottom friction, depends on the surface material and composition of the soil over which the flow occurs. The Manning roughness coefficient represents the resistance to flood flows, so its value is bigger if the soil is rough compared to when it is smooth. In our case, it is important to highlight a significant difference in the parameterization of this coefficient between the floodplain and the river. Floodplains are often fertile due to the sediments transported during floods. As a result, vegetation can grow on these floodplains, increasing flow resistance and, consequently, the Manning coefficient. On the other hand, in rivers, streams, or canals, the consistent flow of water helps smooth the riverbed over time, indicating a lower resistance to flow and contributing to a smaller Manning coefficient. George J. Arcement et al. [16] present a guide for selecting Manning's roughness coefficients for natural channels and floodplains which will be used in this thesis.

The Manning coefficient value in a channel varies principally according to the

base natural material of the soil. It can range from $0.01\frac{s}{m^{1/3}}$ for concrete surfaces to as high as $0.07\ \frac{s}{m^{1/3}}$ for rough soils consisting of rocks and boulder (Tab. 2.1).

Bed material	**Manning base coefficient** n_1
Concrete	0.012 - 0.018
Firm soil	0.025 - 0.032
Coarse sand	0.026 - 0.035
Gravel	0.028 - 0.035
Cobble	0.03 - 0.05
Boulder	0.04 - 0.07

Table 2.1: Manning base coefficient for floodplains and rivers depending on the bed material. Units are in $\frac{s}{m^{1/3}}$.

An adjustment term takes into account various factors such as the bed irregularity, variations in the channel cross-section, presence of vegetation, and other obstruction effects. Furthermore, the Manning coefficient is multiplied by a correction factor that accounts for the presence of meanders, details of the values are shown in Appendix C. This is how we calculate the value of the Manning coefficient in the river :

$$n = (n_1 + n_2)m \tag{2.13}$$

where

- n_1 = a base value depending on bed soil material (Tab. 2.1),
- n_2 = a correction term for additional factors that affect the roughness of the river (Fig C.2),
- m = a correction coefficient for meandering of the channel (Fig. C.2).

In the case of floodplains, the same method is applied but with a vegetation-density additional roughness coefficient :

$$n = (n_1 + n_2)\sqrt{1 + C_* V_{eg_d}(\frac{1.49}{(n_1 + n_2)})^2 R^{\frac{4}{3}}} \tag{2.14}$$

where

- n_1 = a base value depending on bed soil material (Tab. 2.1),
- n_2 = a correction term for additional factors that affect the roughness of floodplains (Fig C.1),

- $C_* =$ an effective-drag coefficient for the vegetation in the direction of the flow,
- V_{eg_d} the vegetation density coefficient,
- $R =$ the hydraulic radius.

This factor specifically accounts for the presence and density of trees and the increased vegetation density within the floodplain, again more details are shown in Appendix C.

Chapter 3

1D-2D models coupling

Now that we have become familiar with both 1D and 2D SLIM models, let's delve into the coupling method itself. Several coupling methods have been presented, we have chosen a coupling method that was deemed the easiest to integrate into the SLIM model. This method, similar to what was previously done in [15], involves coupling the models through a discharge term in the conservation of mass equation. It can be viewed as if each model sees a boundary condition where the 1D and 2D domain meet. This boundary condition imposes a flow depending on the information of the values in the models, a flow that would obviously be the same but with an opposite sign on each side of the boundary. We can therefore already observe that the mass will be conserved, but not the momentum.

In this section, we will first describe the equation used to couple the two models, explaining, in particular, its origin and the assumptions made to justify it. Then we will explain how the 1D and 2D models are geometrically linked, how the equation is incorporated into the mathematical model, and how we will control its use.

3.1 The coupling equation

Our approach involves laterally coupling the 1D and 2D models by adding a discharge source term to the mass conservation equations of both models. We assume that this source term behaves like the flow over a river embankment or protection dikes, which can be described through the weir equation. The weir equation gives us the value of the volume flow rate of a quantity of water passing over a dike or levee as a function of the height of water above that structure.

3.1.1 Demonstration of the weir equation

As described by M.G. Bos. [17], this equation starts from the evaluation of the energy levels of the flow upstream (H_1) and downstream (H) in a control volume around the structure. Assuming that the structure separating the domains is designed to minimize energy losses in the acceleration zone, we can rely on these equations to determine the flow volume. It reads :

$$H_1 = h_1 + \alpha \frac{\overline{v_1^2}}{2g} = H = y + \alpha \frac{\overline{v^2}}{2g}, \tag{3.1}$$

where H_1, H, v_1, v, y, and h_1 are respectively the upstream and downstream energy levels and velocities, the water depth and the water depth over the weir crest (Fig. 3.1). Assuming a uniform distribution of the velocity of water flow, the velocity

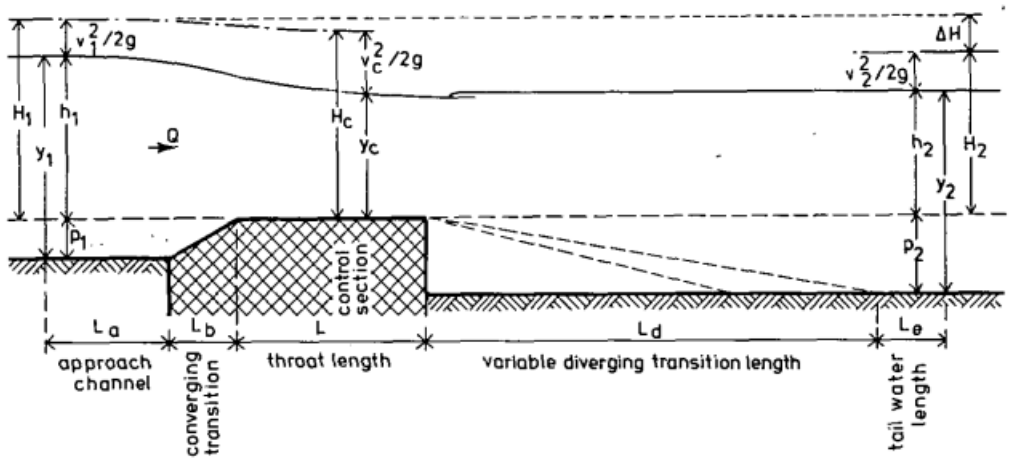

Figure 3.1: Terminology used for the weir discharge equation in [17].

distribution coefficient α is equal to one. We can then find the downstream velocity as :

$$\overline{v} = \sqrt{2g(H_1 - y)} \tag{3.2}$$

By substituting $Q = \overline{v}A$, and given that critical flow occurs at the control section ($y = y_c$), we obtain :

$$Q = A_c \sqrt{2g(H_1 - y_c)} \tag{3.3}$$

Using the criterion for critical flow in a rectangular control section,

$$\frac{\overline{v_c^2}}{2g} = \frac{A_c}{2B_c} = 0.5 y_c \tag{3.4}$$

we have :

$$y_c = \frac{2}{3}H = \frac{2}{3}H_1 \tag{3.5}$$

By substituting this relation and $A_c = y_c b_c$ in Eq. (3.3), we get :

$$Q = b_c \frac{2}{3} H_1 \sqrt{2g(H_1 - \frac{2H_1}{3})} = b_c \frac{2}{3}\sqrt{\frac{2g}{3}} H_1^{\frac{3}{2}} \tag{3.6}$$

To account for the effects of centripetal forces, viscosity, and non-uniform distribution of the velocity coefficient, we introduce the discharge coefficient C_d. The value of this coefficient depends on the shape and type of the measuring structure, which will be discussed further in the thesis.

We approximate the value of the energy head H_1 as the upstream water level over the crest h_1 with this formula: $C_v = [\frac{H_1}{h_1}]^{1.5}$, where C_v is the velocity coefficient, which corrects for neglecting the velocity head at the measurement section and is assumed to be equal to one. Thus, we did not implement it in the equation, but its significance will be discussed later on. We obtain the final formula :

$$Q = C_d \frac{2b_c}{3}\sqrt{\frac{2g}{3}} h_1^{\frac{3}{2}} \tag{3.7}$$

This equation gives us the volume flow rate of water over a protection dike or a levee in our case, depending on the height of water above the structure, h_1. We still need to include the equation in the 1D and 2D mathematical models.

3.1.2 The weir equation in the SLIM model

To incorporate this equation into the source term of the mass conservation using the SLIM model, we must first determine the highest water level η_1 for each boundary, whether it is on the floodplain or in the river. We define η_w as the level of the wall. The upstream water level over the crest h_1 is then given by $\eta_1 - \eta_w$ (Fig. 3.2). To achieve a linear discharge, a discharge that occurs continuously along a line (thus in m^2/s) , we use the following source term :

$$q = C_d \frac{2}{3}\sqrt{\frac{2g}{3}} (\eta_1 - \eta_w)^{3/2} \tag{3.8}$$

According to the SLIM1D mathematical model, the calculated flow rate acts as a new source term in mass conservation equations, as follows :

$$\frac{\partial A}{\partial t} + \frac{\partial Q}{\partial x} = q. \tag{3.9}$$

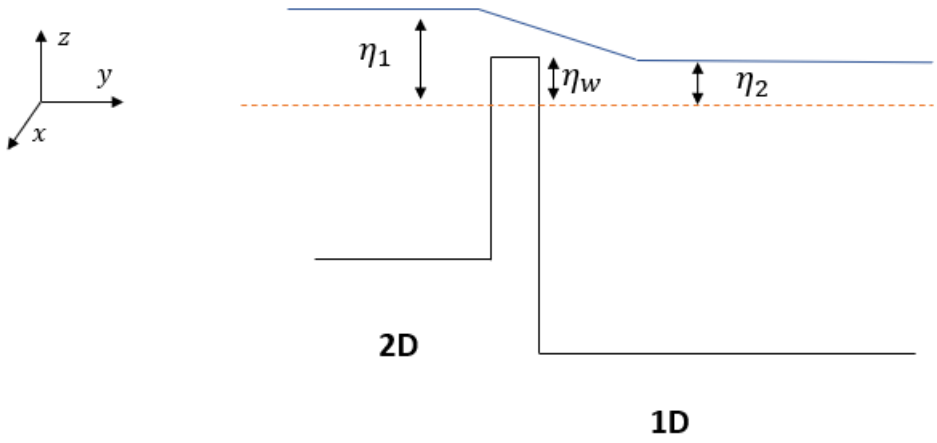

Figure 3.2: Evaluation of the parameters used in the coupled model.

For SLIM2D, the computed flow rate acts as a boundary condition for the segment of the element at the intersection. We can derive this term by writing :

$$\begin{cases} \frac{\partial H}{\partial t} + \nabla \cdot (H\mathbf{u}) = 0 \\ [Hu]_\Gamma = q \end{cases} \tag{3.10}$$

where Γ represents the boundary of an element.

3.1.3 The coupling term with the Discontinuous Galerkin method

The 2D domain is partitioned into N_{2D} triangular elements Ω_e of 3 nodes, while the 1D domain is divided into N_{1D} linear elements, each consisting of two nodes. The domain's geometry comprises a central river modeled in 1D, which is sometimes flanked by a 2D floodplain on either side. At the interface between the river and the floodplains, each 1D node of an element coincides with the two nodes of a neighboring 2D element (see Fig. 3.3). To compute the source term in the 1D equation (3.9) over an element Ω_e, we employ the Gauss quadrature rule :

$$\int_{\Omega_e} q\phi_i dx \approx \sum_{j=1}^{n} q(x_j) w_j \phi_i, \tag{3.11}$$

where n is the number of points, $q(x_i)$ is the discharge at the integration point x_i and w_i is the weight associated with that point. In the 2D equation (3.10), the

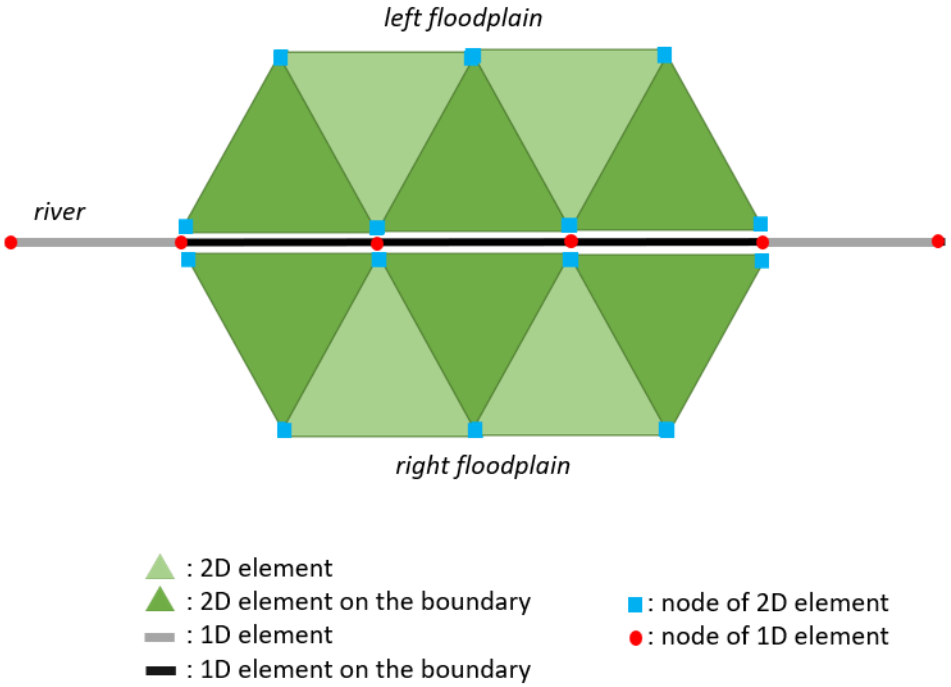

Figure 3.3: Geometry of the coupled scheme.

flow rate acts as a boundary condition for the segments of the elements along the boundary. We formulate the equations around an element in the following manner :

$$\langle \frac{\partial H}{\partial t}\phi \rangle_{\Omega_e} + \langle \nabla \cdot (H\mathbf{u})\phi \rangle_{\Omega_e} = 0, \tag{3.12}$$

which can be integrated by parts :

$$\langle \frac{\partial H}{\partial t}\phi \rangle_{\Omega_e} + \langle \nabla \cdot (H\mathbf{u}\phi) \rangle_{\Omega_e} - \langle Hu \cdot \nabla\phi \rangle_{\Omega_e} = 0, \tag{3.13}$$

finally, Green's theorem gives us :

$$\langle \frac{\partial H}{\partial t}\phi \rangle_{\Omega_e} + \underbrace{\langle \langle Hu\phi \rangle \rangle_{\Gamma_e}}_{=q} - \langle Hu\nabla\phi \rangle_{\Omega_e} = 0. \tag{3.14}$$

3.2 Algorithm of the coupling term

It is now necessary to determine the activation criterion for the coupling source term that has been defined earlier. For example, when the floodplain and the

river are separated by a levee and the water levels of both sides are below the levee, no information exchange occurs, and the coupling source term should thus be turned off. To determine the activation conditions for the coupling source term, we consider the eight different exchange scenarios that may occur between the neighboring nodes of the 1D river and the 2D floodplain (Fig. 3.4).

As a reminder, η represent the relative water level with respect to the equilibrium water level and we use η_{1D} and η_{2D} to denote the water levels at a 1D and 2D node, respectively. To simplify the description and implementation of the coupling, we assign the label η_1 to the higher water level and η_2 to the lower level for each pair of neighboring nodes between the 1D river and 2D floodplain.

$$\eta_1 = max(\eta_{1D}, \eta_{2D}), \quad \eta_2 = min(\eta_{1D}, \eta_{2D}) \tag{3.15}$$

This definition allows us to write the first condition for non-exchange between

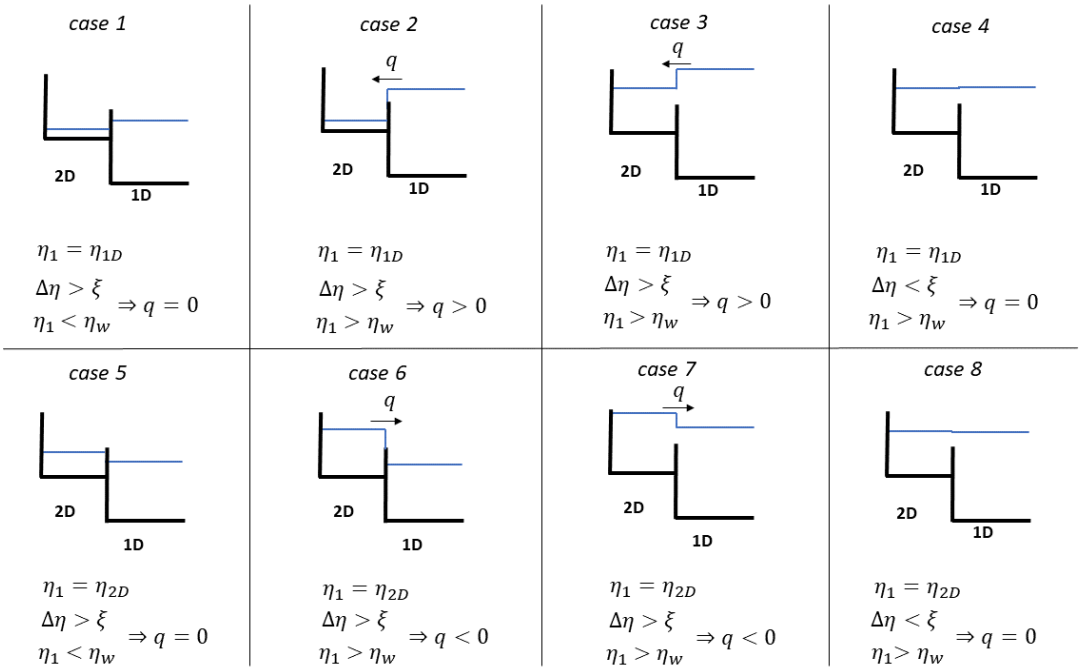

Figure 3.4: Different cases of exchange between the 1D and 2D models, where $\eta_1 = max(\eta_{1D}, \eta_{2D})$, $\eta_2 = min(\eta_{1D}, \eta_{2D})$, $\Delta\eta = \eta_1 - \eta_2$ and $\xi = 10^{-5}m$.

neighboring 1D and 2D nodes. When the difference between the highest and the lowest levels, η_1 and η_2 ($\Delta\eta = \eta_1 - \eta_2$) is small enough so that there is no significant transfer of mass, the water flow must be zero :

$$\Delta\eta < \xi => q = 0 \tag{3.16}$$

Where $\xi = 10^{-5}m$. This scenario corresponds to cases 4 and cases 8 in Figure 3.4. Another condition necessary for mass exchange between neighboring nodes is that the water level exceeds the height of the wall separating the domains. Viewing the wall as a levee, no information is exchanged if the water level does not exceed its height. This scenario corresponds to cases 1 and 5 in Figure 3.4. The condition for this is simply that the highest node level η_1 must be greater than the level of the wall η_w :

$$\eta_1 < \eta_w => q = 0 \tag{3.17}$$

After examining the conditions for no exchange between two neighboring nodes on the boundary, we can now determine the sign of the coupling term. If the highest water level is located in the 2D node, then the coupling term should have a negative sign in front of it, since it is defined as positive when going from the 1D river to the 2D floodplain.

$$if \quad \eta_1 = \eta_{2D} => q = (-1) \times C_d \frac{2}{3}\sqrt{\frac{2g}{3}}(\eta_1 - \eta_w)^{3/2} \tag{3.18}$$

the pseudo-code for activating the source term between two nodes can be summarized as follows :

$\eta_1 \leftarrow \max(\eta_{1D}, \eta_{2D})$
$\eta_2 \leftarrow \min(\eta_{1D}, \eta_{2D})$
$\xi \leftarrow 10^{-5}$
$q \leftarrow 0$
if $(\eta_1 - \eta_2 > \xi)$ **and** $(\eta_1 > \eta_w)$ **then**
  if $\eta_1 == \eta_{2D}$ **then**
    $q \leftarrow C_d \frac{2}{3}\sqrt{\frac{2g}{3}}(\eta_1 - \eta_w)^{3/2}$
  else if $\eta_1 == \eta_{1D}$ **then**
    $q \leftarrow -C_d \frac{2}{3}\sqrt{\frac{2g}{3}}(\eta_1 - \eta_w)^{3/2}$
  end if
end if
return q

3.3 The discharge coefficient C_d

The coefficient of discharge, Cd, is a parameter that corrects for a number of assumptions, straight and parallel streamlines across the head measurement and control section, absence of energy losses between these two sections, and absence of viscous effect. Bos et al. ([17]) parameterize this coefficient based on the shape and type of obstacle existing between the downstream and upstream flow, as well as the

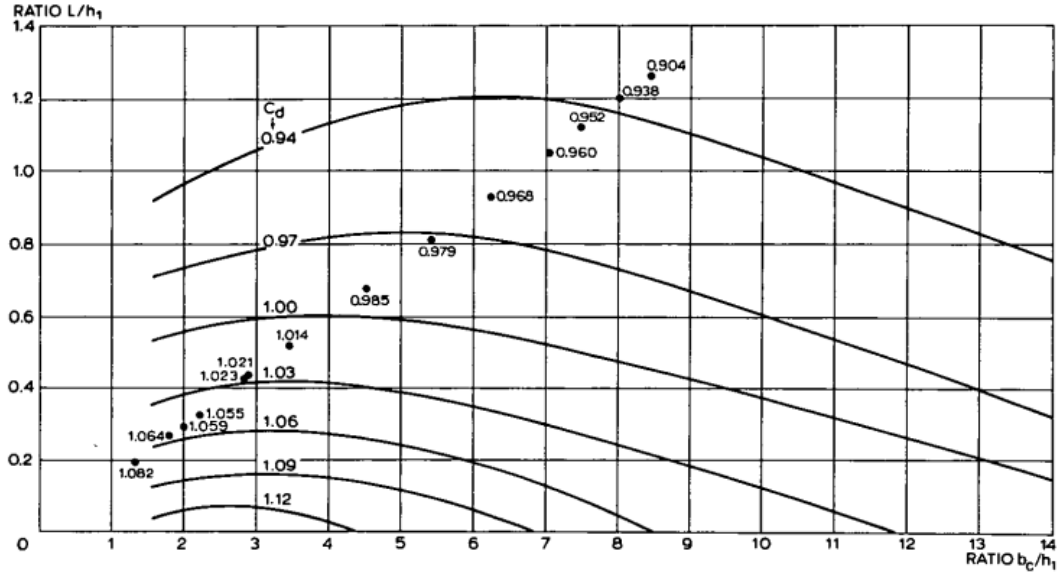

Figure 3.5: Values of the discharge coefficient C_d as a function of b_c/h_1 and L/h_1 [17].

level of energy in the upstream flow. They differentiate between short-crested weirs and broad-crested weirs, also considering sharp-crested weirs. For all these different structures, the discharge coefficient is adjusted to account for the effects it will have on the flow. For example, due to the pressure and velocity distributions above the weir crest, the discharge coefficient of a short-crested weir is higher than that of a broad-crested weir. In our case, it is more challenging to precisely identify the type of structure that will separate the river from the floodplain, as it is variable and can take various forms.

We will assume that the shape of the structure is a short-crested weir. The discharge coefficient will be obtained from Figure 3.5 as a function of the dimensionless ratio $\frac{b_c}{h_1}$ and $\frac{L}{h_1}$, where b_c is the width of the structure, L the length (so here it's assumed to be short) and h_1 the height above the weir crest in the upstream flow. We will assume a value of $C_d = 0.9$.

3.4 Limitations of the model

With this source term added to the mass conservation equations in both the 1D and 2D models, and with the designated conditions for which there would be transfer or not, we have a model that is both fast by the 1D modeling of the river, and accurate by the 2D modeling of the floodplains surrounding it. However, major

limitations can already be highlighted at this point, we will discuss two of them here.

1. Neglecting the momentum transfer between the river and the floodplain dissipates the kinetic energy at the boundary. This raises the question of how significant the kinetic energy transfer is between the river and floodplain, in either direction, in real-life flooding events, and how neglecting it changes the dynamics taking place at these locations.

2. We made the assumption that the discharge behaves like a flow over a weir. Therefore, when the levee size (η_w) is small and the water levels on both sides of the 1D and 2D boundary are significantly higher, the discharge remains the same. This indicates that our model does not account for the significant water level on the other side, which should attenuate the discharge. To address this issue, Bladé et. al [15] propose another coupling equation, that will be introduced in the next section.

3.5 Coupling equation for submerged flows

When the water level from the crest is similar between the upstream and downstream levels, a new discharge term can be derived that takes into account the downstream water level. If we assume that η_1 is the highest water level and η_2 the lowest, Bladé et. al [15] suggest the following :

- If $\frac{2}{3}(\eta_1 - h_w) > (\eta_2 - h_w)$, then the discharge q is given by :

$$q = C_d \frac{2}{3}\sqrt{\frac{2g}{3}}(\eta_1 - h_w)^{3/2}, \tag{3.19}$$

- If $\frac{2}{3}(\eta_1 - h_w) < (\eta_2 - h_w)$, then the discharge q is given by :

$$q = C_d\sqrt{2g}(\eta_1 - h_w)(\eta_1 - \eta_2)^{1/2}. \tag{3.20}$$

By using these equations, the source term becomes less significant when the water levels on both sides are close, and it remains the same as before otherwise. This term will not be used in the results of the thesis but will serve as a discussion for further exploration.

Chapter 4

Results

In this section, we will go through the various tests that were conducted as the method progressed, aiming to identify the specific physical features that are incorporated into our model, but also the main positives and negative points of the method, using a fully 2D reference model. Although the reference model does not precisely represent the fluid motion one might encounter in a laboratory or field case, it serves as a benchmark for assessing the accuracy of the model.

- The first test serves as a verification of mass conservation, aiming to determine if the total volume remains the same in a closed system and if it returns to equilibrium after a disturbance. This test is crucial for assessing the system's ability to maintain mass balance and recover its original state after perturbations.
- The second test involves three different 2D reference models, and by comparing them with our coupled model, it helps identify the reference model that yields the most similar results. Selecting the reference model that closely aligns with the behavior and outcomes of the coupled model, aids in understanding the physical features of our model and determining which setup is the most reliable.
- The purpose of the third test is to simulate a more realistic flow by introducing specific features into the model. By comparing the simulations of the coupled model and the reference model, we can identify the influence of our method on the flow dynamics. This test aims to assess how our method affects the flow behavior and dynamics compared to the reference model.

4.1 Mass conservation assessment

We consider first a simple test case to assess whether our model conserves the total mass of the fluid. In a closed system, two floodplains each with an area of $8m^2$ are situated alongside an $8m$ long and $2m$ wide river (Fig. 4.1).

- The upper floodplain, or left floodplain has a water head level of $2m$, resulting in an initial volume of $V_{fp1} = 2 \times 8 = 16m^3$,
- The right floodplain has a water head level of $2.5m$, resulting in an initial volume of $V_{fp2} = 2.5 \times 8 = 20m^3$.
- The river has a head of $3m$, resulting in a volume of $V_{r_{in}} = 3 \times 16 = 48m^3$.

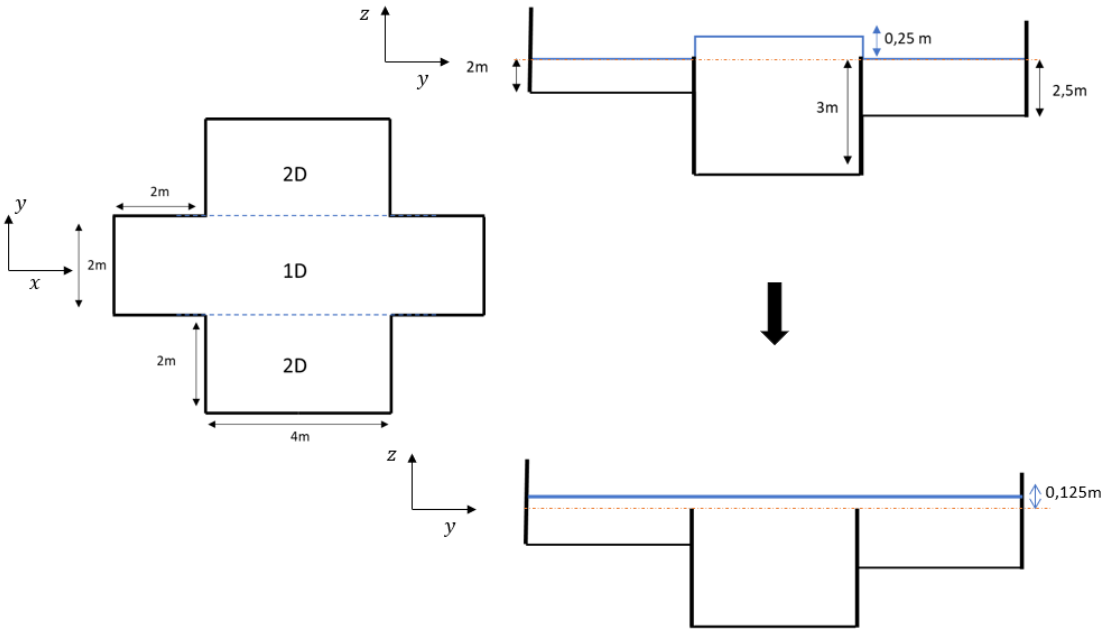

Figure 4.1: Scheme of the mass conservation assessment test case.

The mesh of the 1D and 2D coupling is visible using Paraview, a data visualization tool, as shown in Fig. 4.2. Initially, the river is elevated by $0.25m$, causing it to overflow into the floodplains in order to balance the system. As a result, there is a surplus volume in the river of $V_s = 0.25 \times 8 = 4m^3$ that must spread out over a total surface area of $A_{tot} = 8 + 8 + 16 = 32m^2$. Therefore, at equilibrium, the final water level must reach $\eta = \frac{V_s}{A_{tot}} = 0.125m$ throughout the entire domain.
The final volume in the floodplain and the river should be :

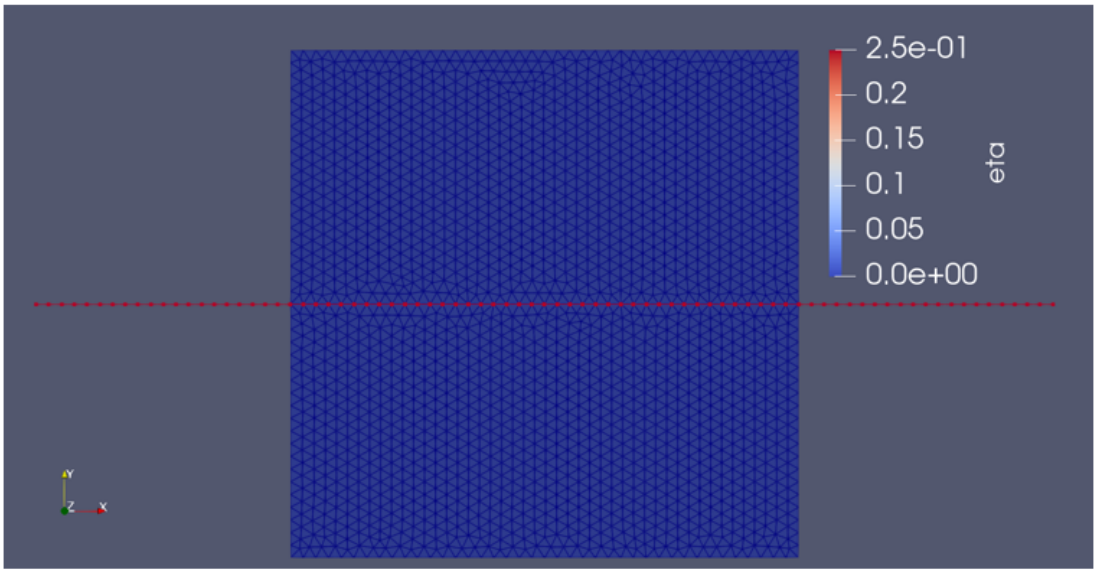

Figure 4.2: Screenshot of the test case in Paraview at $t = 0$, showing η on the domain ranging from 0 to $0.25m$. The 1D river is represented by the dotted red line, and the 2D floodplains are the blue rectangular area composed of triangular elements.

- $V_{fp} = V_{fp1} + V_{fp2} + 0.125 \times 16 = 36 + 2 = 38m^3$,
- $V_r = V_{r_{in}} + 0.125 \times 16 = 48 + 2 = 50m^3$.

After 10 s of simulation with a time step of $\Delta t = 0.001s$, the volumes on the river and floodplains were integrated, and the values converged to the predicted ones (Fig. 4.3).

The total volume over the domain was also integrated, indicating that no mass was created (after 1950 iterations, the total volume changed by $1.7 \times 10^{-12}m^3$). The same test has been conducted using the submerged flow equation (Eq. 3.20) and is available in appendix B of the report (Fig B.1).

4.2 Tests for Comparison of Mass and Energy

Having established the accurate mass conservation in our coupled model, we will now focus on comparing our coupled 1D-2D model with a fully and directly constructed 2D model, without any coupling. This 2D model replicates the geometry and the specified conditions of our coupled model. Our objective is to examine the difference between the 2 models across 3 different configurations and identify the configuration that produces the most similar results between the coupled model

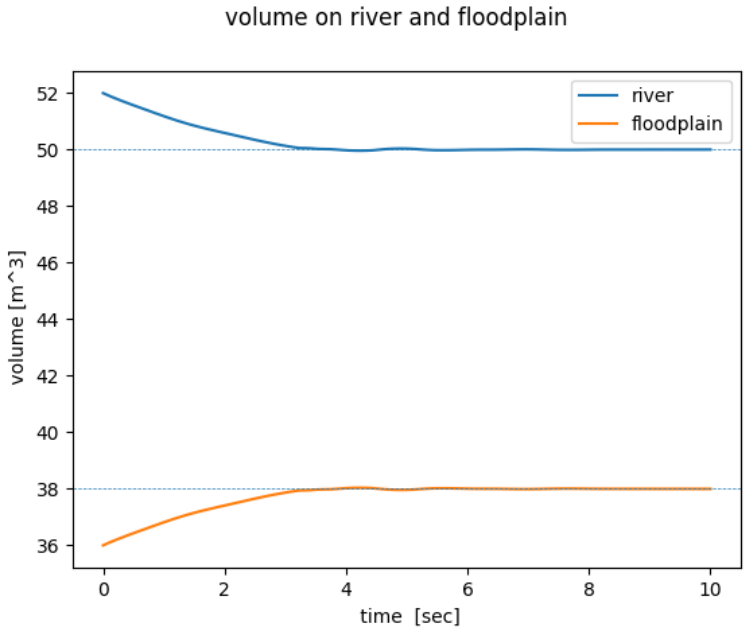

Figure 4.3: Plot of the volume on the river and floodplain in the coupled model.

and the full 2D model. To visualize the differences among the models, we will focus on the transfer of mass and kinetic energy across the 1D-2D boundary. We will compare the changes in energy and mass in both the river and floodplain, while also plotting water levels at specific intervals.

The 3 test configurations are similar to the one used to verify mass conser-

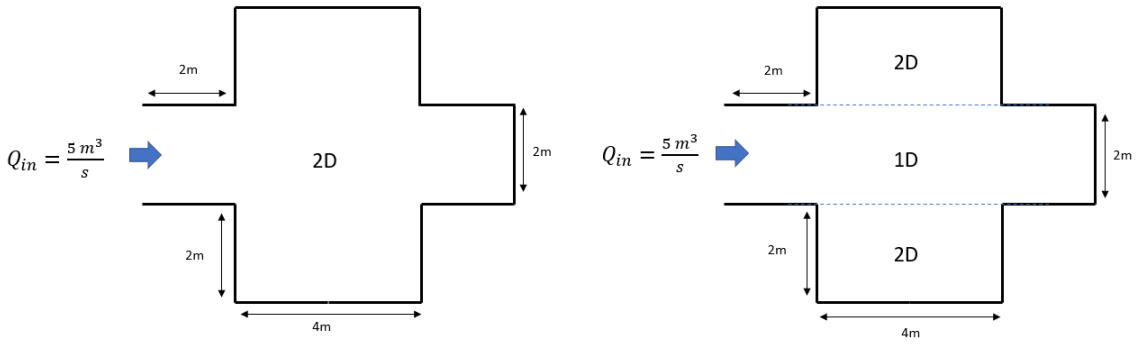

Figure 4.4: Scheme of the second test. On the left is the full 2D model, and on the right is the coupled 1D-2D model.

vation in the previous section. It consists of a straight 1D river spanning 8m in length, with two 4m-long and 2m-wide floodplains situated alongside. However, the floodplain bathymetry is now 1m, and the inlet boundary has been modified to maintain a constant flow rate $Q = 5m^3/s$. The entire basin has an initial water level $\eta = 0m$. At the end of the river, a wall is placed to visualize water reflections (Fig. 4.4).

In the previous sections, we demonstrated the numerical implementation of a wall between the 1D and 2D models using the weir equation in our simulation. However, it is important to note that this barrier is considered infinitely thin in the numerical model, whereas in reality, such a structure cannot physically exist. Therefore, we will investigate the influence of this wall on fluid dynamics by constructing three comparative full 2D models. Each model represents a different scenario regarding the presence of a physical structure resembling the wall between the river and the floodplain. The cross-sectional views of the three models are depicted in Fig. 4.5 and are described as follows :

i) The first model is constructed without any walls or levees between the river and the floodplains. In the coupled model, we assign a value of $-1m$ to η_w.

ii) The second model is built with a thin wall (0.05m wide and 0.7m high) between the river and the floodplains. In the coupled model, we assign a value of $-0.3m$ to η_w.

iii) The third model includes a thick wall (0.2m wide and 0.7m high) between the river and the floodplains. The value of η_w in the coupled model is also assigned as $-0.3m$.

To compute the amount of kinetic energy in a specific part of the domain, we integrate the following formula using the relevant data :

$$E_{kin} = \int \frac{|\mathbf{u}^2|\rho}{2} dV \tag{4.1}$$

To determine the water level in the river, we average the values along a straight line using an integral, obtaining the average water level over the length of the river :

$$H_{river}(x) = \frac{1}{2w} \int_{-w}^{w} H(x, y) dy \tag{4.2}$$

where w represents the width of the river. The same process is applied to the floodplain, but in this case, we calculate the water level along a longitudinal strip of approximately 0.5m width.
We will conduct simulations using a time step of $\Delta t = 0.001s$ for a duration of

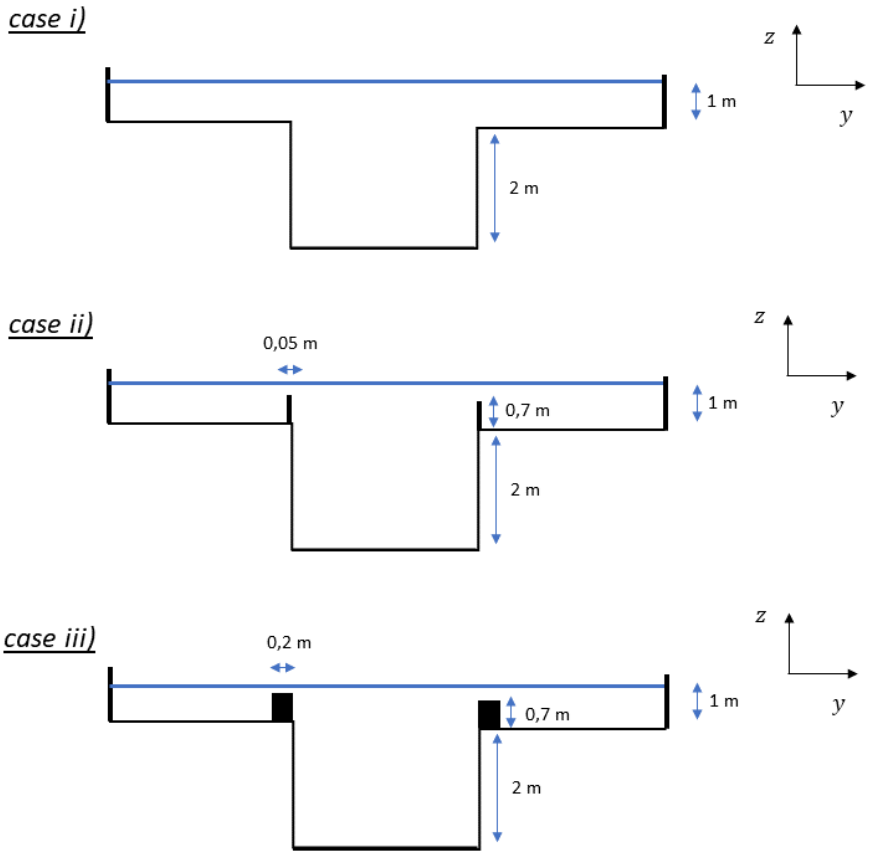

Figure 4.5: Cross-sectional view of the basin, the blue line represents the level of water. Case i) is the test case without a wall between the river and the floodplain, case ii) represents the test case with a thin wall, and case iii) represents the test case with a thick wall.

3 s. This time interval allows us to observe the behavior of the initial wave as it propagates, bounces against the wall at the end of the river, and propagates back. For each test case, our analysis will focus on the variation of the water height at $t = 1s$ and $t = 2s$ within the strip of the floodplain and the river. We will also present screenshots from ParaView, displaying the surface representation of η in the complete 2D model at the corresponding time instances.
Additionally, we will investigate the variations in mass and kinetic energy within the river and the floodplain. These analyses will provide valuable insights into the dynamics of the system with the different structures composing it.

4.2.1 case i) with no wall between floodplain and river

The first model represents the scenario without any walls or levees between the river and the floodplains. In this configuration, we assign a value of $-1m$ to η_w, indicating that the discharge will be more important between the 1D and 2D models (see Eq 3.8).

The comparison of water heights provides several interesting insights (Fig 4.6). Firstly, at $t = 1s$, we observe that the water height in the river is approximately 5 cm higher in our coupled model compared to the full 2D model, while in the floodplain, the water level in our coupled model is about 5 cm lower than what is expected in the full 2D model. Another noteworthy point is that at a distance of 2 meters in the x-direction, in the floodplain graph, there is a depression where the water level drops by around a dozen centimeters. We can observe this phenomenon in the ParaView screenshot, where we can identify the dark blue area corresponding to this lower water level. This effect is not present in the coupled model, suggesting that it originates from the inertia and momentum effects in the full 2D model, possibly a recirculation zone.

Regarding the 2-second period, we notice a minor difference in water height between the two models, as well as a reduction in the magnitude of the "depression" mentioned earlier. Regarding the evolution of volume (Fig 4.7), we can observe that although it follows a similar trend in both models, there is a slight difference of just under 2 m^3 at 1.5 s. Additionally, there is a noticeable discrepancy of approximately half in the estimation of kinetic energy in the floodplain, highlighting the significance of momentum conservation in the coupling process.

4.2.2 case ii) with the thin wall between the floodplain and the river

The second model represents the scenario with a thin wall of 0.7 meters-high, along the river separating it partially from the floodplains. In this configuration, we assign a value of $-0.3m$ to η_w, indicating that the discharge between the 1D and 2D models will be less important than in the case (i) (see Eq. 3.8). By examining the water height graph after $1s$ (Fig 4.8), we can observe that the two heights are closer together in this configuration compared to when no walls are present between them. However, the presence of a depression zone in the floodplain is still noticeable, particularly in the floodplain height plot at a distance of 2 meters in the x-direction. This observation is further supported by the ParaView screenshot, where we can see that the depression has shifted toward the edge of the floodplain due to the presence of the walls.

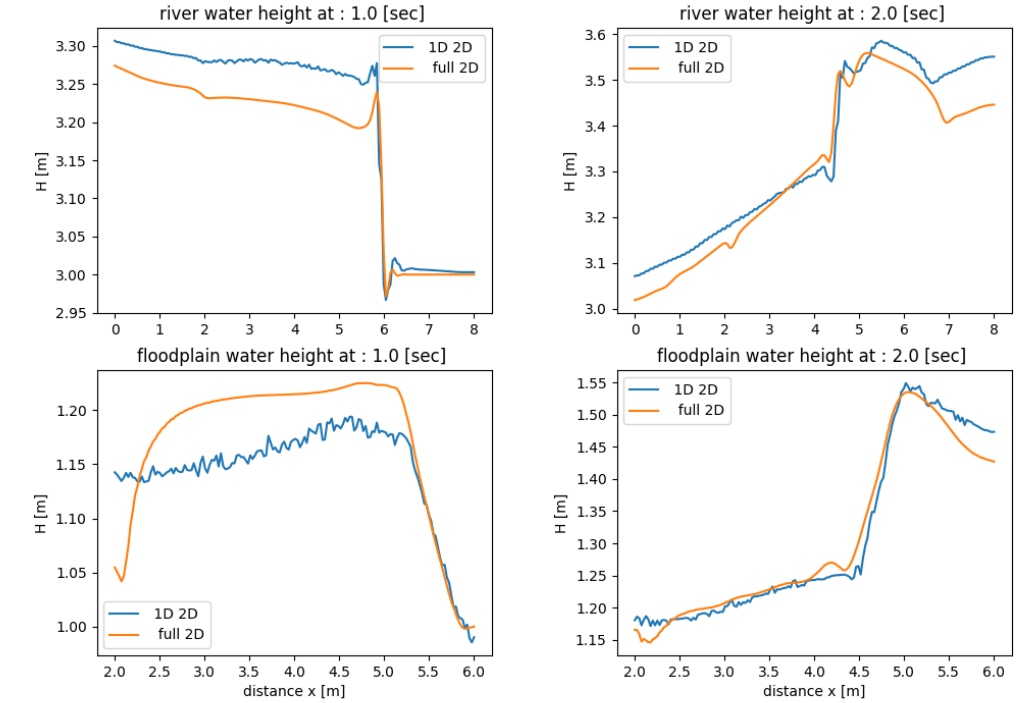

(a) (b)

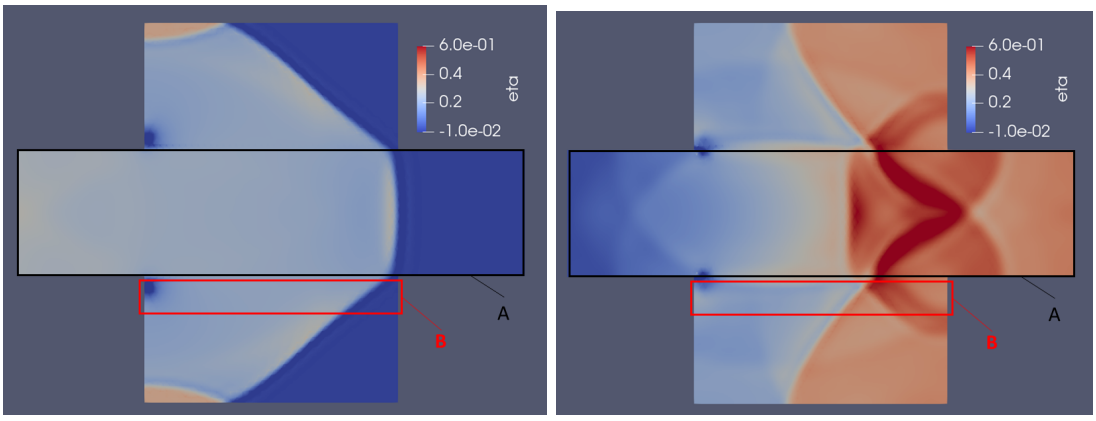

(c) (d)

Figure 4.6: Case (i) with no wall between the river and the floodplain :
(a) water height at 1s in a strip of the floodplain (Zone B) and the river (Zone A),
(b) water height at 2s in a strip of the floodplain and the river,
(c) ParaView screenshot of the water surface elevation (η) in the full 2D model at $t = 1s$,
(d) ParaView screenshot of the water surface elevation (η) in the full 2D model at $t = 2s$.

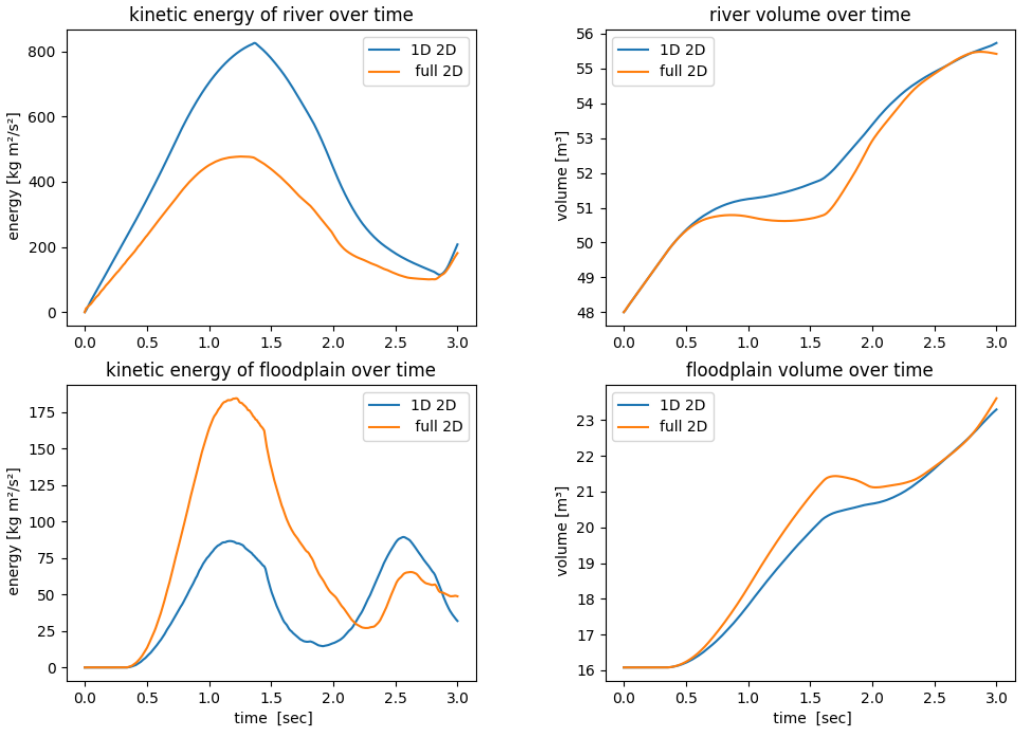

(a) (b)

Figure 4.7: Case (i) with no wall between the river and the floodplain:
(a) the evolution of kinetic energy in the floodplain and in the river,
(b) the evolution of volume in the floodplain and in the river.

Regarding the mass evolution (Fig 4.9), a significant improvement can be observed, as the two curves no longer differ by 1 m^3 at 1.5s, and their levels become more equal towards the end of the simulation. The addition of these walls in the 2D model has led to a decrease in the kinetic energy level within the floodplain. As a result, the two curves have become closer to each other.

4.2.3 case iii) with a thick wall between the river and the floodplain

The third model corresponds to a scenario with a thick wall, measuring 0.2 meters in width and 0.7 meters in height, partially separating the river from the floodplains. In this configuration, we assign a value of $-0.3m$ to η_w, indicating that the discharge between the 1D and 2D models will be less significant compared to case (i) (see Eq. 3.8). The influence of wall thickness has been discussed in the section on the discharge coefficient C_d, where a thicker wall implies a lower discharge coefficient. We have not changed the discharge coefficient between case (ii) and case (iii) because the value of 0.9 remains correct for this wider structure. We still expect that with a thicker wall, the volume in the floodplain in the full 2D model will be smaller than with a thin wall. There is no noticeable difference in water height (Figure 4.10) between the thick wall and the thin wall.

Regarding the evolution of mass and energy (Figure 4.11), as expected, we observe that there is less volume of water on the floodplains due to the reduced discharge resulting from the larger wall.

4.2.4 RMSE of river water height for the three cases

By showcasing the changes in volume and kinetic energy and the water height at different times, we can highlight the physical differences occurring in the simulation across the 3 cases. The purpose of the conducted tests, however, was to determine which structural configuration yields more similar results between the coupled model and the full 2D model. To accomplish our initial objective, we will calculate the root mean square error (RMSE) of volume in the river for each scenario, between the coupled model to the full 2D model (Fig. 4.12) :

$$RMSE(t) = \sqrt{\overline{(V_{1D2D}(t) - V_{f2D})^2}} \tag{4.3}$$

Where $V_{1D2D}(t)$ and $V_{f2D}(t)$ represent respectively the river water volume in the coupled model and in the full 2D model. This figure accurately reflects what we had identified previously. We can observe that the configuration without a wall

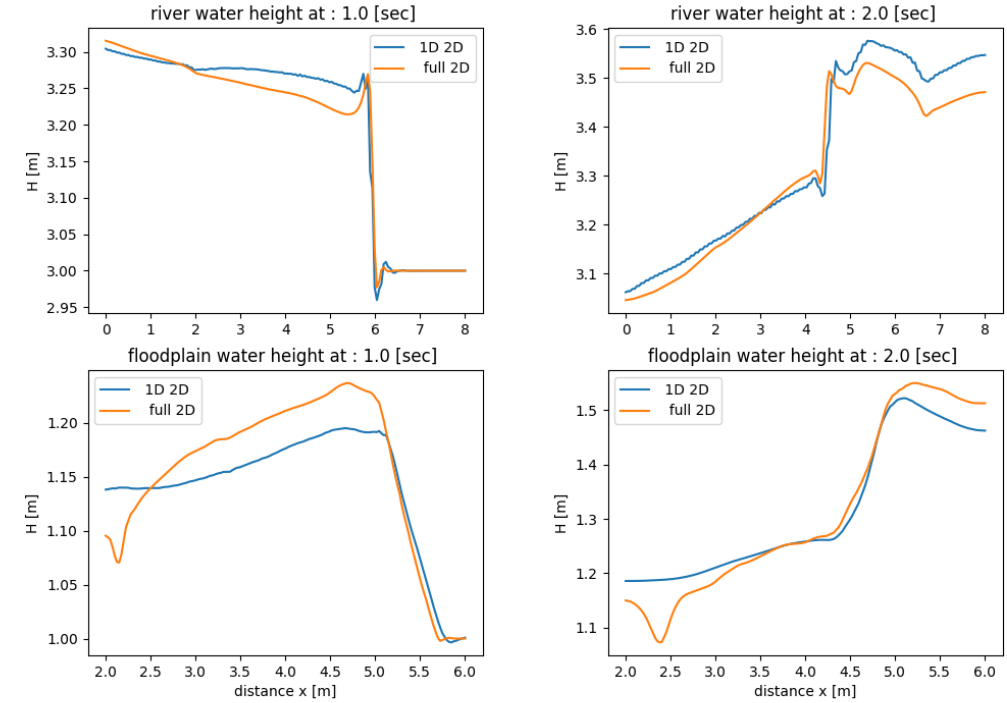

(a) (b)

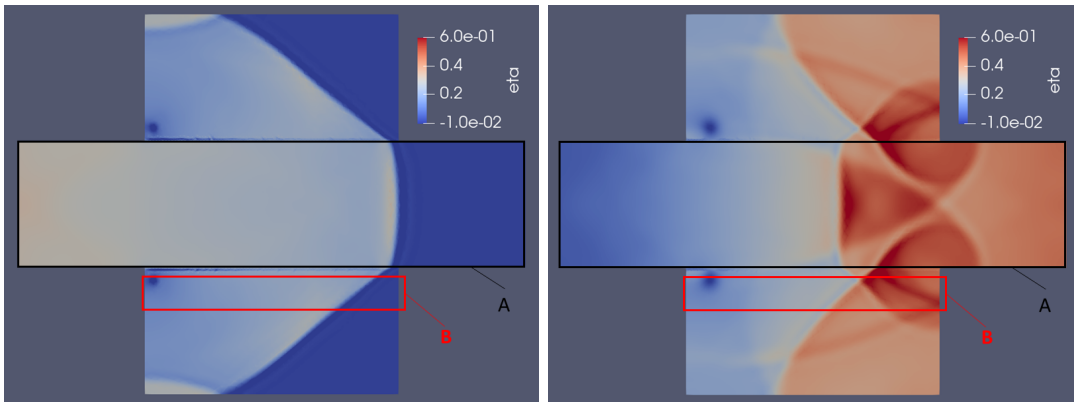

(c) (d)

Figure 4.8: Case (ii) with a thin wall between the river and the floodplain :
(a) water height at 1s in a strip of the floodplain (Zone B) and the river (Zone A),
(b) water height at 2s in a strip of the floodplain and the river,
(c) ParaView screenshot of the water surface elevation (η) in the full 2D model at $t = 1s$,
(d) ParaView screenshot of the water surface elevation (η) in the full 2D model at $t = 2s$.

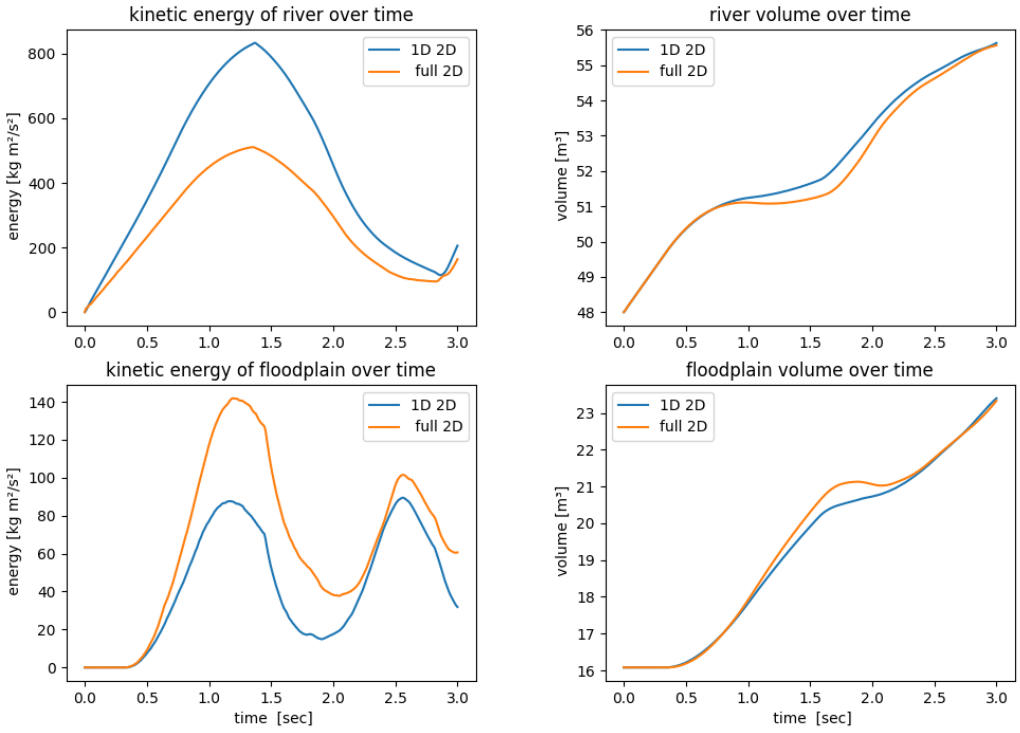

(a) (b)

Figure 4.9: Case (ii) with a thin wall between the river and the floodplain :
(a) the evolution of kinetic energy in the floodplain and in the river,
(b) the evolution of volume in the floodplain and in the river.

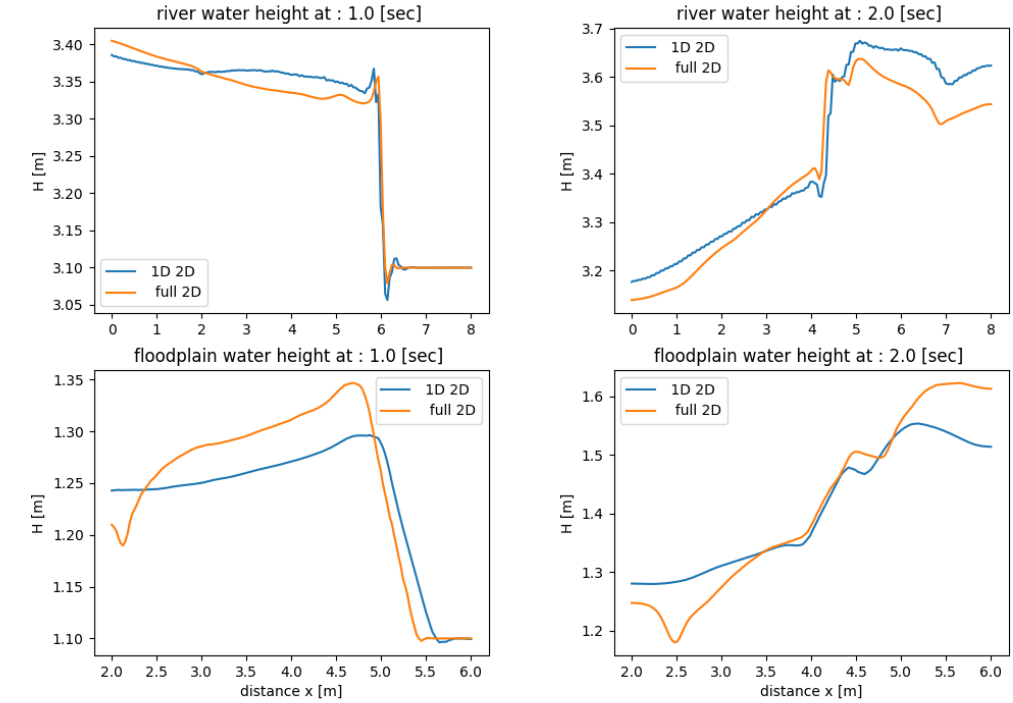

(a) (b)

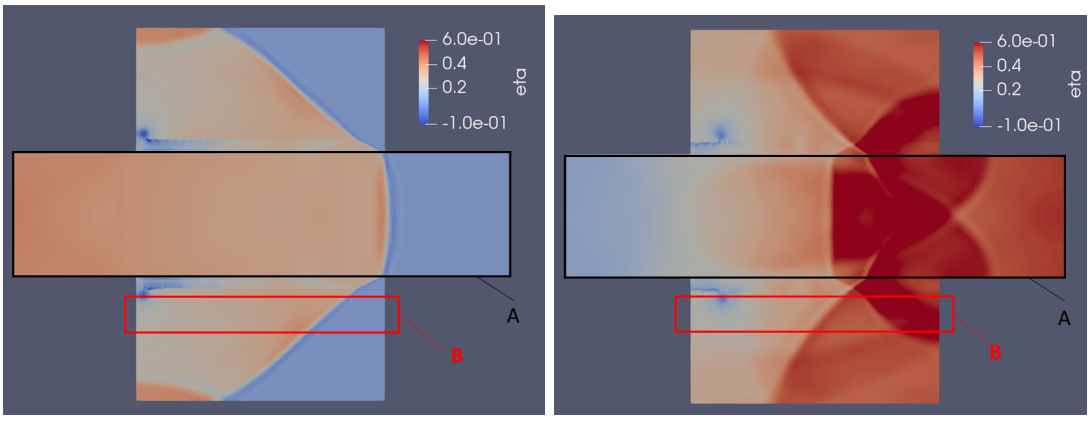

(c) (d)

Figure 4.10: Case (iii) with a thick wall between the river and the floodplain :
(a) water height at 1s in a strip of the floodplain (Zone B) and the river (Zone A),
(b) water height at 2s in a strip of the floodplain and the river,
(c) ParaView screenshot of the water surface elevation (η) in the full 2D model at $t = 1s$,
(d) ParaView screenshot of the water surface elevation (η) in the full 2D model at $t = 2s$.

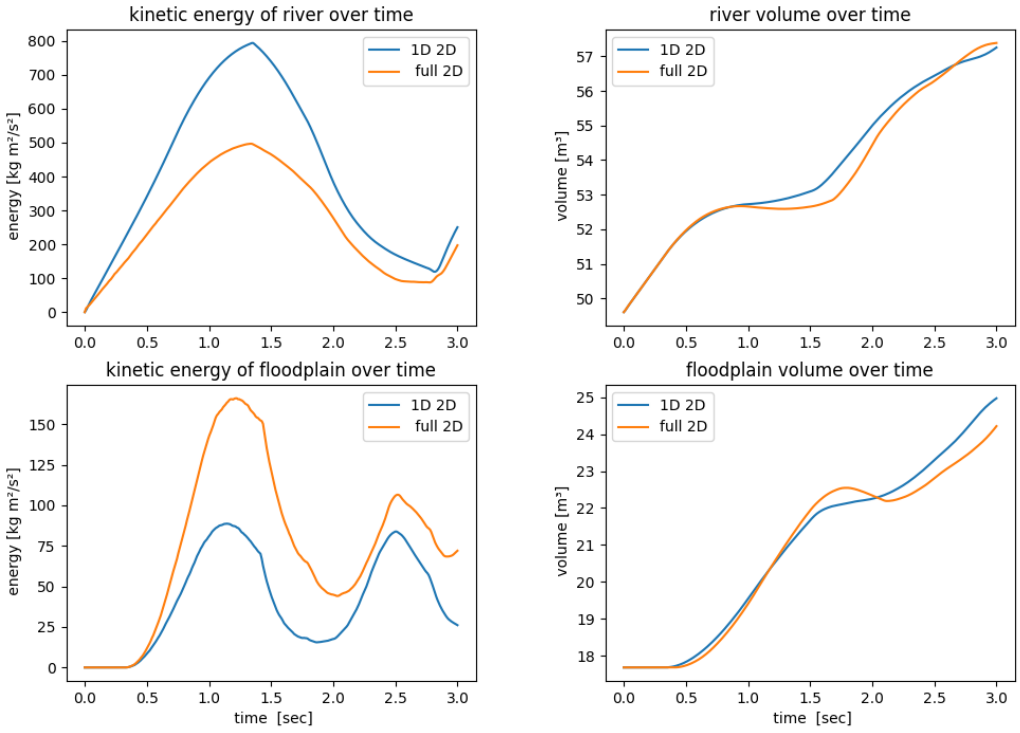

(a) (b)

Figure 4.11: Case (iii) with a thick wall between the river and the floodplain :
(a) the evolution of kinetic energy in the floodplain and in the river,
(b) the evolution of volume in the floodplain and in the river.

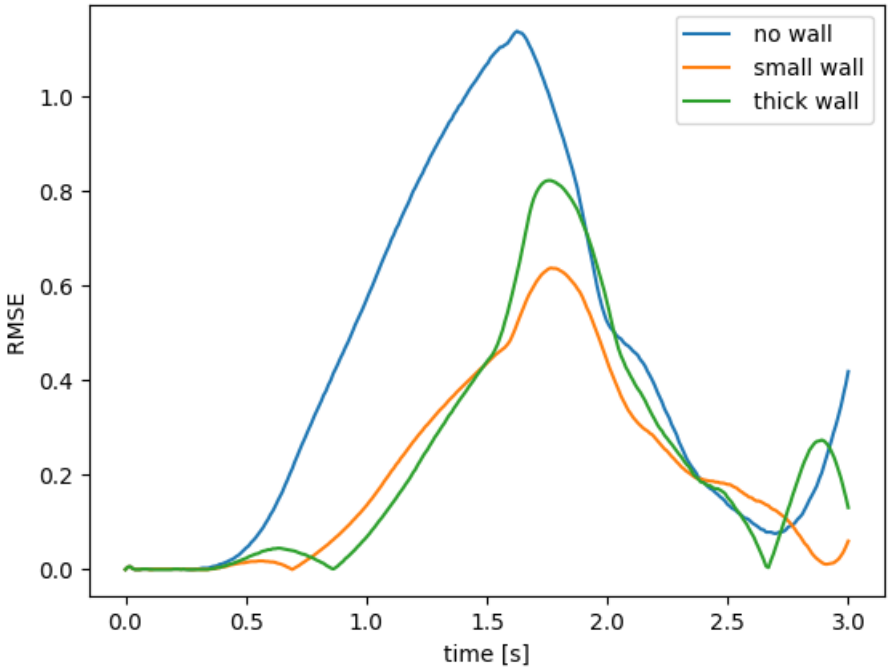

Figure 4.12: Root mean square error of the river volume for the 3 configurations test case.

produces less accurate results compared to the other two, with an error of over $1m^3$ at 1.5s. The difference between the two models with a wall is less distinct, although there is a smaller peak for the case with a small wall.

These three cases have demonstrated the importance of the wall's presence in the models, primarily in relation to both mass and kinetic energy transfer. The existence of the wall diminishes the exchange of kinetic energy between the floodplain and the river, consequently leading to reduced errors in the models. This improvement is attributed to the coupled model effectively dissipating all kinetic energy at the boundary. Furthermore, we were able to observe the absence of depression zones (or recirculation zones) in the coupled model, which is a direct result of the momentum transfer across the 1D-2D boundary. However, it is worth noting that the overall volume error between the models remains relatively small. At its maximum, there is a difference of $1m^3$ for a total volume of slightly less than $80m^3$ at 1.5 s.

4.3 Test case : Wetting and Drying Algorithm

We will proceed with a more comprehensive example in order to observe the model results under laboratory-like conditions, using the same simple bathymetry including the presence of a thin wall between the river and the floodplains.

- The global level of water will initially decrease to reach the level of the levee after $10s$, followed by a discharge in the main channel that raises the water level in the river and spreads into the floodplains, starting at $15s$.
- To ensure the drying of floodplain nodes and elements, we need to incorporate the explicit Wetting and Drying Algorithm. This algorithm allows us to have nodes with a water height of 0 by using limiting values in the SLIM2D terms, where the denominator is the water height.
- Additionally, we will include the bottom friction term using the Manning-Stickler formula, which was not implemented in the previous tests. As discussed in the respective section, the Manning coefficient represents the resistance to flood flows, and it will be higher in the floodplain compared to the river. We will parameterize this coefficient in both environments based on assumptions regarding the composition of their soils.
- While maintaining the overall size and shape of the test domain, we will introduce a lateral slope in the floodplain towards the river (see Fig 4.13).

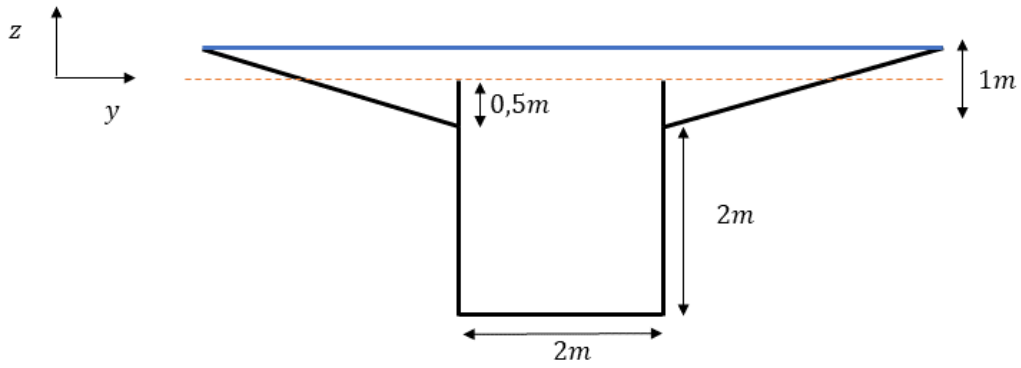

Figure 4.13: Cross section of the geometry used in the Wetting and Drying test. The blue line is the initial water level, the orange dotted line represents the $\eta = 0$ level.

To ensure stability in the simulation, we will start by emptying the domain and establishing a stable state at the level of the levee. Instead of starting with empty nodes, we will impose a gradually decreasing water level at the outlet boundary until it reaches the level of the wall (Fig. 4.13). Subsequently, we will introduce

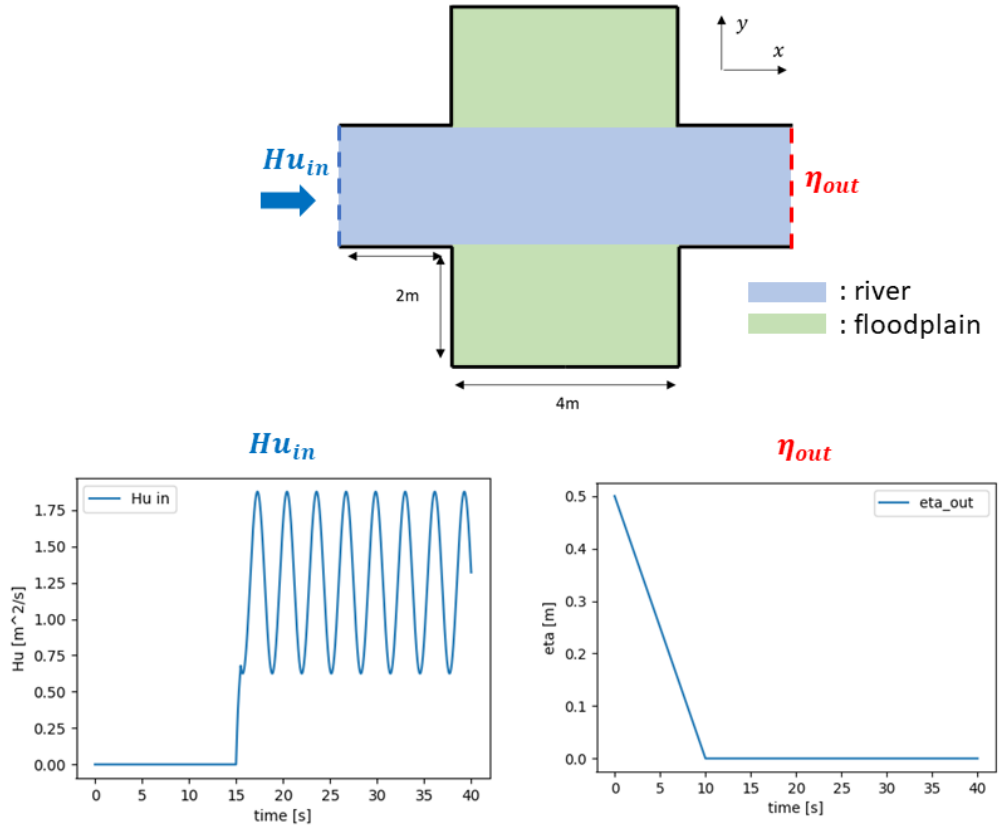

Figure 4.14: Condition imposed in the Wetting and Drying test case. The upper figure is an upper view of the domain. The graph on the left is the inlet boundary condition imposing a sinusoïdal velocity transport. The graph on the right represents the outlet boundary condition imposing a gradually decreasing level of water.

a sinusoidal flow rate at the inlet and analyze changes in mass and energy across different parts of the domain. Furthermore, we will discuss the computational time required for both the full 2D model and the 1D-2D model. In order to calculate the potential energy, we use :

$$E_{pot} = \int_{\Gamma} \rho g \frac{\eta^2}{2} dxdy \tag{4.4}$$

Where Γ is the surface of the domain, $\rho = 1000kg/m^3$ is the density of water, $g = 9.81m/s^2$ the earth's gravity and η represents the relative water level with respect to the equilibrium water level. This will provide us with a value of potential energy relative to the equilibrium water level $\eta = 0m$.

4.3.1 Manning coefficient

For the Manning coefficient, we will consider a smooth concrete river ($n_1 = 0.02\frac{s}{m^{1/3}}$) without any additional adjustment factors. Using equation (2.13), we can calculate the coefficient as follows:

$$n_{river} = (n_1 + n_2)m = 0.02\frac{s}{m^{1/3}} \tag{4.5}$$

The computation of the Manning coefficient for the floodplain is made using equation (2.14). We will assume a cobble soil ($n_1 = 0.05\frac{s}{m^{1/3}}$) with a moderate degree of irregularity and a large amount of vegetation and obstructions ($n_2 = 0.15\frac{s}{m^{1/3}}$). Additionally, we will consider a vegetation density of $Veg_d = 0.005$ and an effective drag coefficient of $C_* = 11$. The hydraulic radius is calculated as $R = \frac{2\times4}{4+8}m$. With these values, we can compute the Manning coefficient for the floodplain as follows:

$$n_{fp} = (0.05 + 0.15)\sqrt{1 + (11 \times 0.005) \times \left(\frac{1.49}{0.2}\right)^2 \times 1.31^{\frac{4}{3}}} \approx 0.5\frac{s}{m^{1/3}} \tag{4.6}$$

4.3.2 Results

When comparing the evolution of volume in the floodplain and the river, we observe that during the first 10 seconds of "emptying" the basin by gradually imposing an outflow boundary condition of -0.5 m, both models closely follow the same trajectory. Subsequently, when a sinusoidal flow rate is imposed at 15s, the volumes remain quite similar, with a maximum difference of $0.5m^3$ in the river. This can be explained by the fact that during the domain emptying process, the water level reaches the same height as the wall ($\eta = \eta_w$). Therefore, we obtain the ideal configuration for applying the equations of the weir, which explains why the 2D system and our coupled system exhibit such close behavior in this configuration.

Regarding the kinetic energy in the river, the error between the models is significantly reduced compared to previous tests. Instead of having an energy that is twice as high in the river, we observe a notable improvement, with a maximum difference of approximately 25% at around 18s. This improvement is attributed to the configuration where the communication space between the floodplain and the river is significantly reduced. The presence of the wall effectively blocks the lateral

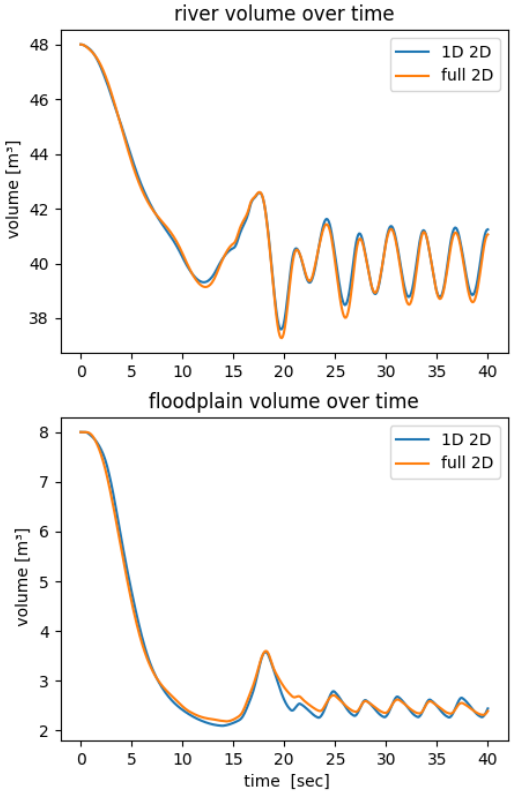

Figure 4.15: Evolution of volume in the river and left floodplain for the Wetting and Drying case, for the coupled model and the full 2D model.

transmission of kinetic energy, which is predominantly preserved within the river. We can see that the transmitted kinetic energy in the floodplain remains much lower in magnitude compared to the values obtained in the river, where it does not exceed 25 J of kinetic energy. The potential energy of the flow is generally more significant than the kinetic energy.

The last comparison in this section pertains to the simulation time. The mesh used for the floodplains in both the full 2D model and the coupled model is the same, consisting of 5976 triangular elements, with finer resolution near the river border. Using a time step of $\Delta t = 0.001s$ in an explicit scheme with 40000 iterations, the CPU time for both models is shown on Table 4.1.
We observe that the computation time is approximately 1.8 times faster with our

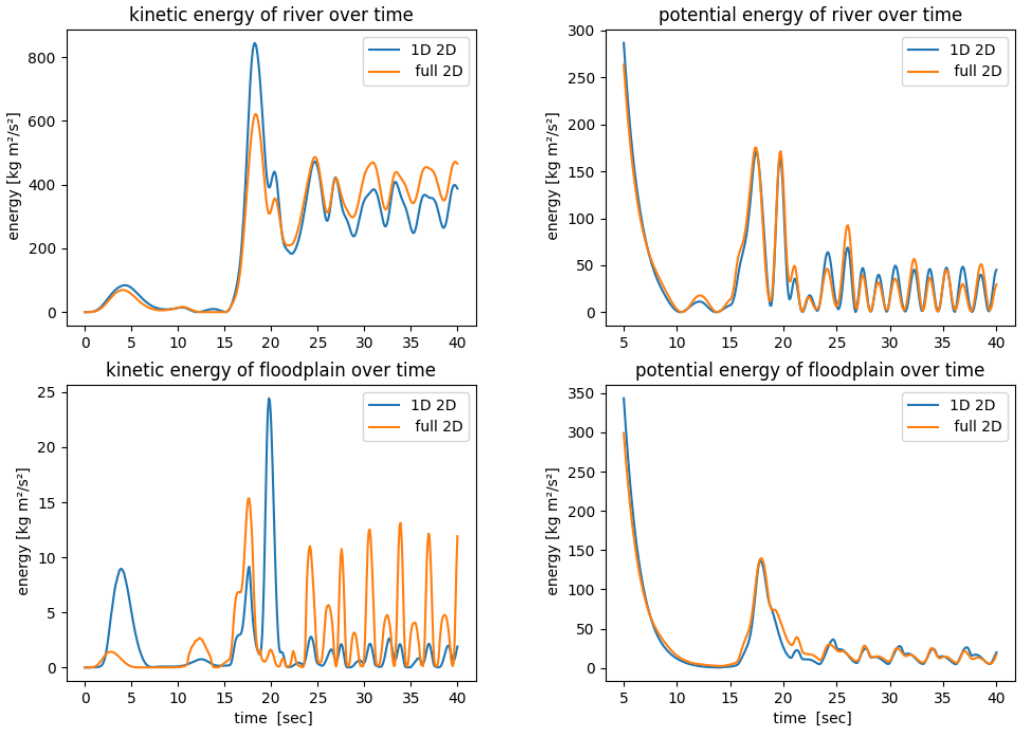

(a) (b)

Figure 4.16: Evolution of kinetic energy (a) and potential energy (b) in the river and left floodplain for the Wetting and Drying case, for the coupled model and the full 2D model.

model	CPU time [*sec*]	number of 2D elements	number of 1D elements
1D 2D	546	5976	124
full 2D	950	11134	0

Table 4.1: CPU time and elements required for the Wetting and Drying test.

coupled model than with the full 2D model.

4.4 Discussion

In this section, we first identified the reference model that yielded the closest results to our coupled model. This model includes a thin wall between the floodplain and

the river, resembling a near-perfect configuration for applying the weir equation, which calculates the flow rate over a weir based solely on the water height above the wall. By establishing this structure, we significantly reduce the amount of momentum transferred from the river to the floodplain, bringing us closer to the coupled model, which does not transmit any momentum. Through the analysis of water heights at different time steps, the overall flow dynamics conservation is confirmed, with noticeable differences attributed to momentum effects. Regarding the second test, it confirms that in a longer simulation involving additional factors, similar conclusions can be drawn.

However, it is important to note that this approach is relevant primarily for the purpose of identifying the ideal reference model that aligns well with our coupled model. Firstly, the configuration of the model, which incorporates a thin wall of constant size along the river, is not commonly found in literature tests on simple surfaces. Secondly, the reference model is based on the equations of SLIM2D, which is still a numerical representation of the 2D flow and lacks certain details that real-world flows possess, such as the Wetting and Drying Algorithm that imposes a water height limit. On the other hand, the floodplains in both models are modeled using the same equations and algorithms, hence the similarities observed in their behaviors.

To validate the model using these tests based on simple bathymetry, it would be necessary to conduct measurements using a laboratory-scale case. As discussed in several of the methods presented in the introduction, laboratory cases using simple surfaces have been conducted ([12], [18] ,[15]) . Due to time and resource constraints, these tests were not carried out. However, for future work, it would be entirely possible to replicate the configurations and conditions of one of the tests mentioned here in order to compare our data with those from the corresponding experiment. In this case, comparing the equation of the weir used here with the equation for submerged flow (Eq. 3.20) can help us identify which one produces more realistic results.

While our tests may not be as revealing as a laboratory experiment, certain interpretations and discussions can still be drawn. As mentioned in the introduction, the transfer of momentum is discussed in several coupling methods. The data obtained from these tests provide us with evidence to support this claim, and the impact of kinetic energy can be discussed. Despite a disparity in the calculated kinetic energy between the two models, they both conserve mass in a similar manner, thus limiting the impact of momentum transfer in the study of floodplain volumes. As we have seen in the introduction, Kuiry et al. [14]

accurately calculate the flooded area in a real-world situation without applying momentum conservation, or even velocities in the floodplain. These results allow us to question the actual impact of momentum transfer in a coupled model when considering variables such as the flooded area of a river or the volume spread along its banks. Furthermore, we can observe that a significant portion of the total energy in the floodplain is potential rather than kinetic, and the magnitudes involved in calculating potential energy are much larger. This comparison with potential energy further raises questions about the impact of kinetic phenomena in floodplains.

Concerning the time computation, the coupled model finished iterating 1.8 times faster than the reference model. This is due to the fact that the 2D river requires calculations in two dimensions, which are more time-consuming compared to the 1D modeled river. The 2D river consists of more than 5000 elements, while our simple 1D modeled river is represented by 124 1D elements. Naturally, it is expected that the computation time is longer for the 2D river compared to the 1D river. However, it is also interesting to observe the influence of the additional coupling step in the equations forming the 1D-2D model on the computation time. We can conclude that this additional step does not have as much impact on the computation time as the 2D meshing of the river. It should be noted that these timing tests were conducted on my computer without utilizing any standardization method. Nevertheless, these values still give us an idea of the effective speed of the coupled model. The other models presented also show significantly reduced computation times. Kuiry et al. [14] achieved results six times faster with their coupled model compared to the full 2D model.

The advantage of this laboratory-like test was to obtain precise results under controlled conditions and ensure the consistency of the two models. However, its limitations lie in the interpretation of results for more complex and realistic conditions and phenomena. In the next section, we will apply the model to a more realistic case to further enrich the discussion with additional findings.

Chapter 5

Realistic model comparison

5.1 The bifurcation test case

Now that we have presented the different stages of model construction through comparative tests, we will focus on a much more realistic scenario: the case of a bifurcation. This complex geometry will allow us to assess the model's relevance in studying real river floods. As discussed in the introduction, river flooding is a growing problem and the need to study their behaviors is crucial. The JRC report suggests that the construction of retention areas is an effective measure to prevent flood damages, as it mitigates peak flows during floods. Therefore, when evaluating the applicability of our model in flood studies, our primary interest shifts from analyzing kinetic and potential energy to calculating the river discharge, aiming to obtain a value that is truly useful for risk analysis and flood damage assessment.

The domain consists of a rectangular floodplain with dimensions of 600m in width and 1000m in length, intersected in its center by a 'Y'-shaped river. The river has a width of 40m and a depth of 15m. Upstream, the river is a straight line that bifurcates into two rivers of equal cross-section after 600m. This division occurs in the middle of the floodplain, with each river branch forming a 30° angle with the initial straight line. The two river branches then exit the floodplain at the corners of the rectangular area (Fig. 5.1). Along the entire course, there is a slight longitudinal slope of 0.01%, and a lateral slope in the floodplains naturally directs the flow of water toward the river. For a width of 280m, the floodplains gradually rise to a height of 10m at the other end, creating a lateral slope of 3.3% (Fig. 5.2). We assume the Manning coefficient for the river and floodplain to be the same as in the previous test, $n_{fp} = 0.5$ and $n_r = 0.02$.

Similarly to the previous test, the entire domain is initially submerged. To

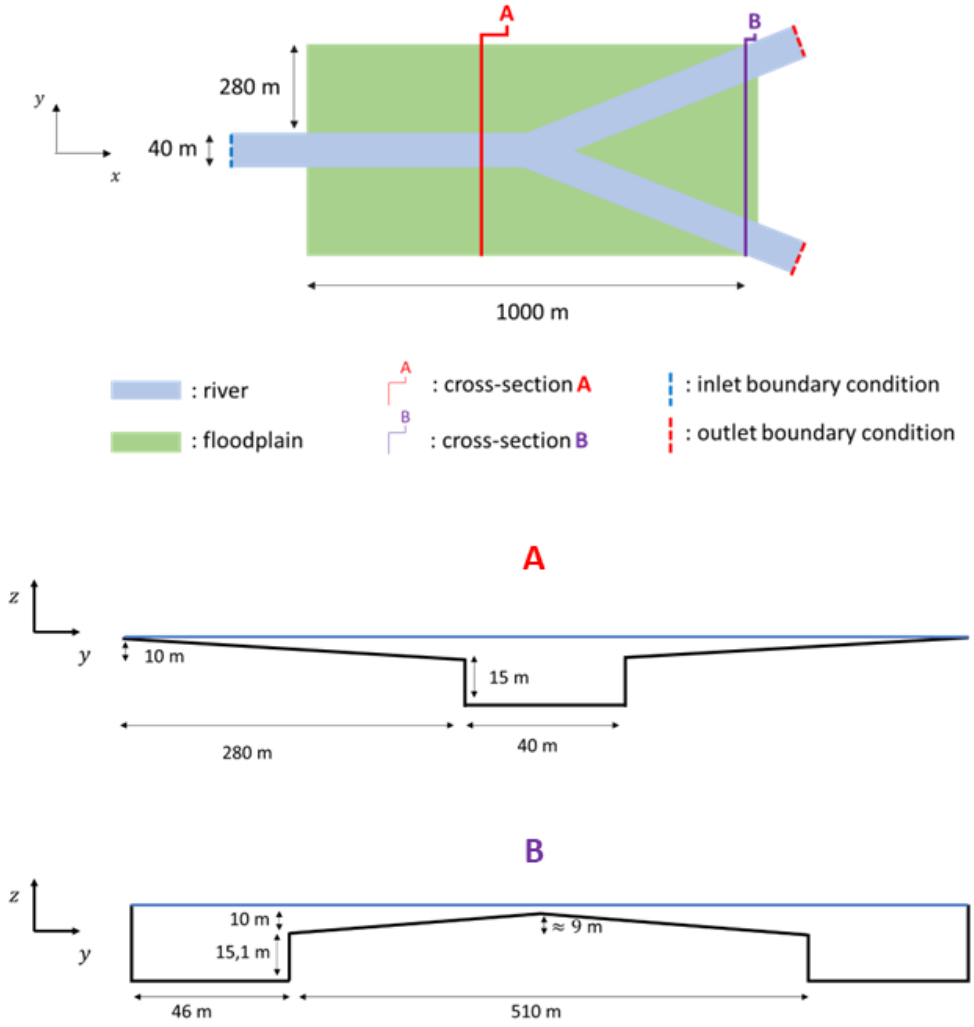

Figure 5.1: Geometry of the bifurcation. The first figure is the upper view of the domain, with the location of two cross-section views, A and B. The figure in the middle represents the cross-section A, upstream of the bifurcation and the figure below represents the cross-section B, downstream of the bifurcation.

reach a situation where the floodplains are dry, we apply a decreasing outlet boundary condition on the water level η. On both outlet boundaries of the separated rivers, the water level will decrease from $\eta = 10m$ to $\eta = 0m$ in less than 40 minutes. After this recession period and a stabilization time of 2000s, a significant inflow of water gradually enters the upstream river, reaching for 15 minutes a discharge

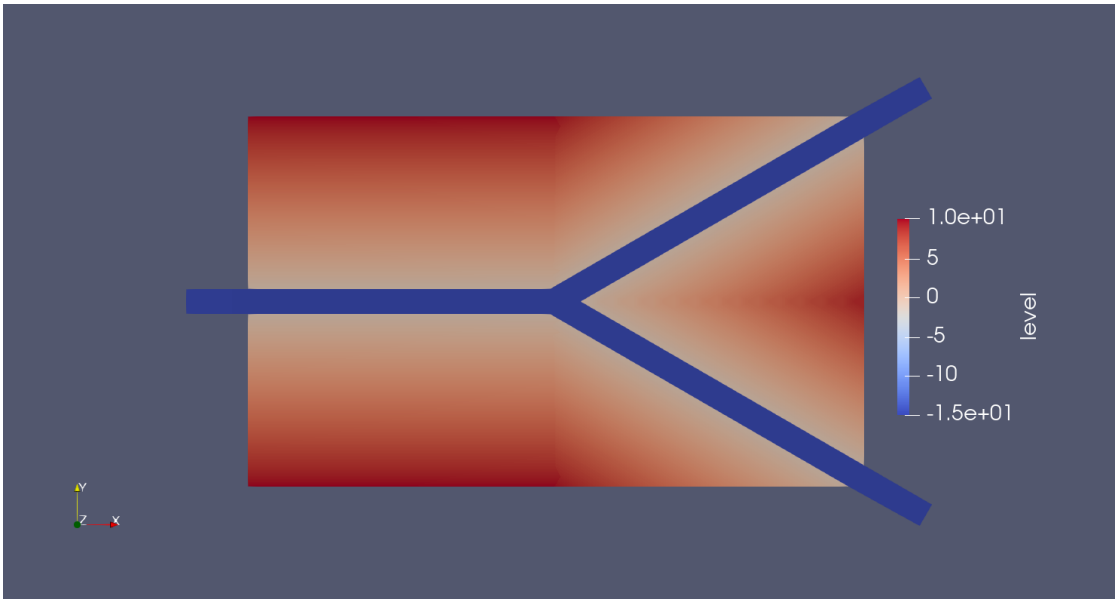

Figure 5.2: upper-view of the bifurcation domain using Paraview. Elevation in the river is set to -15 m in dark blue, and elevation in the floodplain is ranging from 0 to 10 m high (red).

of 2500 m^3/s, which corresponds to a flow transport velocity of 60 m^2/s (see Fig. 5.3). The input flow then attenuates to return to a stable situation.

Our analysis will therefore focus on studying the discharge at the upper outlet section and in a section of the river upstream of the bifurcation, and also to examine the influence of a significant change in river direction on the difference between both models' evolution of volumes.

5.2 Results

By examining the river discharge right before the bifurcation, so in the upstream straight river (Fig. 5.4), we can initially observe a first peak, resulting from the initial recession of the basin. We won't delve into this part in detail as it primarily serves the purpose of drying the floodplain. Starting from 4000s as the discharge increases in the river due to the boundary condition, we can observe that the coupled model reaches a discharge close to the inlet discharge of 2000 m^3/s, while the reference model obtains a $200m^3/s$ lower discharge, reduced by the dissipation of kinetic energy on the floodplain. For the rest of the simulation, the discharges remain close, as already observed in similar configurations during the previous test.

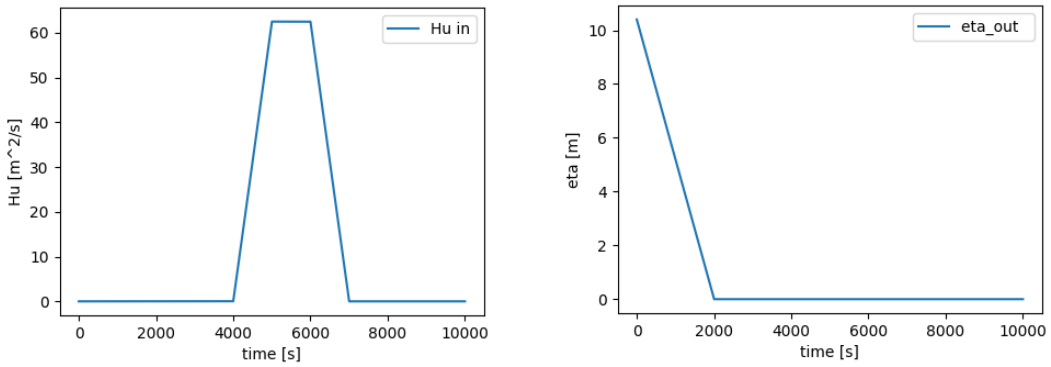

(a) (b)

Figure 5.3: Boundary conditions of the bifurcation. (a) The inlet transport velocity, (b) outlet conditions regarding the level of water η.

When examining the calculated discharge at the end of the flow, in the left branch near where we imposed the boundary condition (Fig. 5.5), several interesting points are worth noting.

- First, we can observe that the discharge resulting from the boundary condition starting at 4000s has significantly decreased (from $2000m^3/s$ to $1000m^3/s$). This is explained by the separation of the river, but also that a portion of the kinetic energy dissipated during the turn.
- Furthermore, the difference the discharges between the two models throughout the simulation is more noticeable than for the pre-bifurcation discharge (Fig. 5.4). This difference in discharge can be explained by the transmission of momentum between the river and the floodplain during the change in river direction. Indeed, when the river flow reaches the bifurcation in the reference model, its inertia and momentum cause it to spread across the floodplain in front of it. Leading to dissipation in kinetic energy, and thus reducing the discharge in the river. However, in our coupled model, there is no distinction between a lateral or more frontal boundary; the only exchange between the river and the floodplain occurs based on water levels, thereby failing to transmit a portion of the energy and momentum that should be distributed and dissipated over the floodplain.

Overall, the river discharge is fairly well represented by our coupled model, with a maximum error of 15% during the peak at the outlet.

We will also analyze the volume evolution in the floodplain and the river to

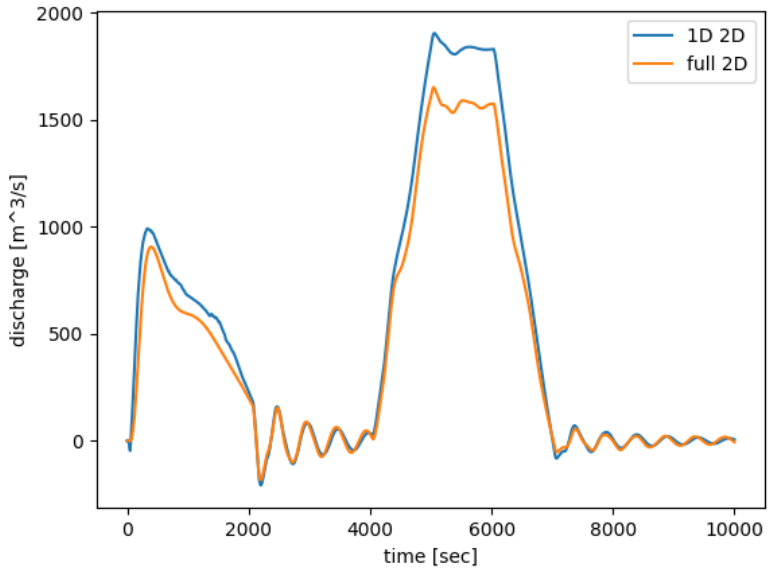

Figure 5.4: Evolution of the discharge on a section of the river upstream of the bifurcation (near cross-section A on Fig. 5.1) for the coupled and the reference models.

complement the analysis with additional insights. For the evolution of volume (Fig. 5.6), the tool used to compute the volume error between the two models is the Mean Absolute Percentage Error (MAPE) calculated as follows:

$$MAPE(t) = \left| \frac{V_{f2D}(t) - V_{1D2D}(t)}{V_{f2D}(t)} \right| \times 100\% \tag{5.1}$$

where $V_{f2D}(t)$ is the volume in the 2D model and $V_{1D2D}(t)$ the volume in the coupled model. Data before 2000 seconds are not shown for the sake of clarity and result relevance.

For the river, we can observe a consistent vertical shift throughout the simulation between the two models in the evolution of the river volume. The hypothesis proposed to explain this difference is a similarity issue between the two models. Indeed, a certain amount of water may have been neglected in the simplification of the 1D river model, either at the bifurcation or due to inaccuracies in slope calculation or channel length. By comparing the initial river volume difference between the two models at $t = 0s$ and at $t = 2000s$ when the floodplain volume is dried up, we do observe a discrepancy that can explain this vertical shift.

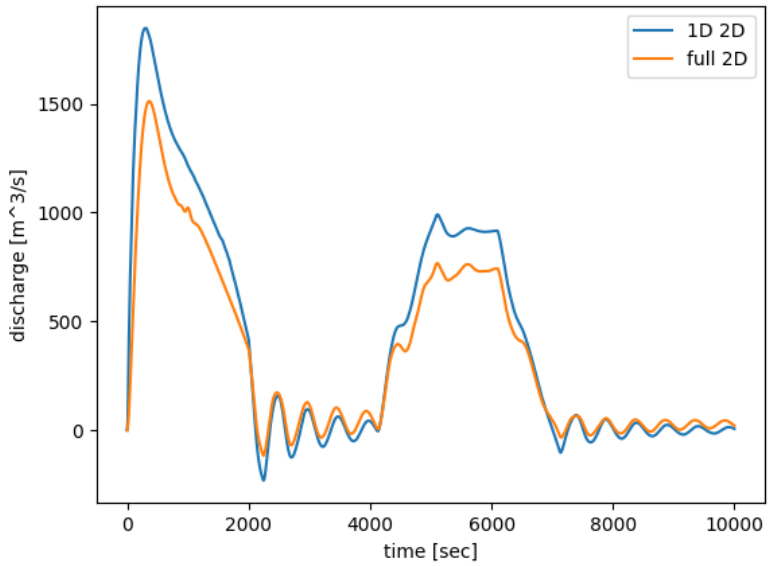

Figure 5.5: Evolution of the discharge on a section of the left river downstream of the bifurcation (near upper cross-section B on Fig. 5.1) for the coupled and the reference models.

- At $t = 0$s the volume difference between the rivers in the two models is $44000m^3$ (2.1% difference).
- At $t = 2000$, the volume difference between the rivers in the two models is $31000m^3$ (2.5% difference).

We thus computed the evolution of the river volume shifted from the difference at $t = 2000s$, revealing a remarkable similarity between the volumes (Fig. 5.6). This explains why the derivative of this volume, the discharge, was not influenced by this constant shift. It is essential to note that this adjustment is purely informative, and caution should be exercised when relying on such an approach. When examining the error between the models, it can be observed that it varies around 2.5%, and in the case where we shifted the coupled model, the error significantly decrease, reaching a maximum of 0.4%.

Regarding the floodplain, the coupled model consistently shows significantly smaller volumes (Fig. 5.6). The error reaches 17% between 6000s and 7000s (when the inlet discharge decreases). Two reasons could explain this significant difference :

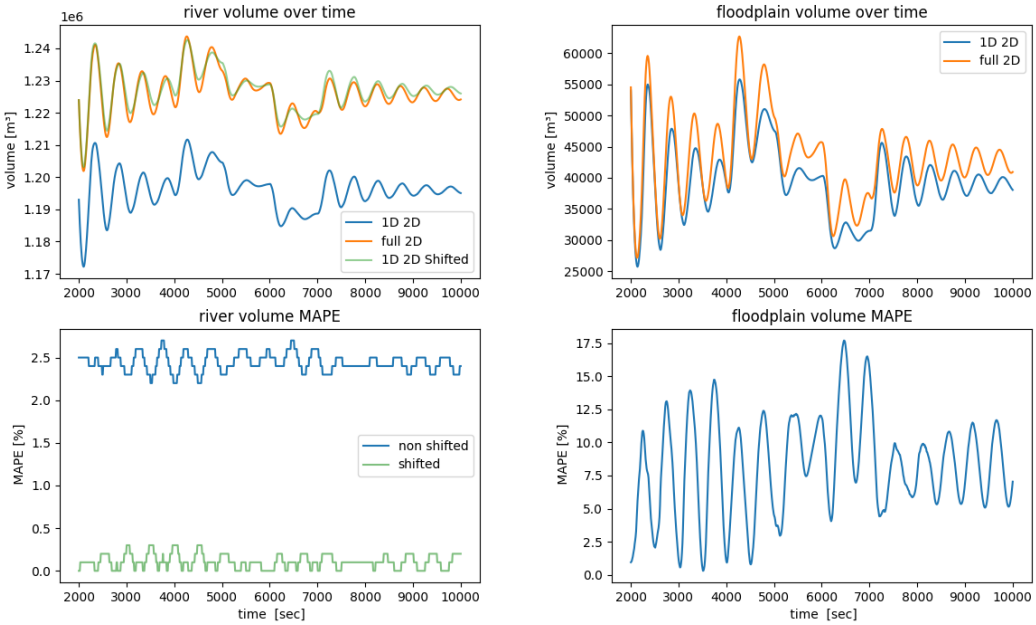

(a) (b)

Figure 5.6: (a) Upwards, the evolution of water volume in the river for the reference, coupled, and coupled corrected (shifted) models. Downwards, the Mean Absolute Percentage Error (MAPE) between the reference and coupled models, and between the reference and coupled corrected models.
(b) Upwards, the evolution of water volume in the floodplain for the reference and coupled models. Downwards, the Mean Absolute Percentage Error (MAPE) between the reference and coupled models.

- The bathymetry of the floodplain in the coupled model does not perfectly match that of the full 2D model. Due to the complexity of the floodplain's geometry and the way it has been implemented, some areas are not exactly similar in both models, principally along the river edges after the bifurcation.
- The non-conservation of momentum in the coupled model, and more precisely due to the presence of the bifurcation. When the flow encounters the nodes that are oriented more frontally at the turns, a portion of the longitudinal momentum is transmitted into the full 2D model but not into the coupled model.

Upon examining the time aspect (Tab. 5.1), we can observe that there is hardly any time-saving. This can be explained by the significance of the floodplain size in this case. Since the floodplain is large compared to the size of the river, the number of 2D elements in both models is very similar. Therefore, the computation time is dominated by the 2D floodplain portion, and the time saving is not significant in this scenario. However, it could be more significant in cases where the 2D river represents a larger size, as we have seen in the previous test.

model	CPU time [*sec*]	number of 2D elements	number of 1D elements
1D 2D	1978	3640	102
full 2D	1981	3779	0

Table 5.1: CPU time and elements required for the bifurcation test.

5.3 Discussion

By introducing complex bathymetry, we faced an additional challenge in successfully integrating the models, which is evident in the obtained mass results. In the literature, the real cases scenario are often focusing on the study of flooded areas. This parameter carries more significance and relevance than the overall volume evolution on the floodplain, as it can be easily compared with satellite data collected in the field and indicates the extent of flooding influence surrounding the river. For future work, it would be interesting to focus on this surface rather than mass and compare it with field data ([14]).

But our analysis also focuses on a phenomenon that has not been addressed in the presented schemes, which is the river discharge. As demonstrated by previous studies [2] [19] , accurately simulating the river discharge is crucial for assessing potential risks. By analyzing the data related to river discharge, we can further

evaluate the performance of our coupled model and its usefulness in flood studies. Solutions such as the construction of retention areas and the conservation of floodplains are designed to reduce peak flow in a river, therefore, knowing the accurately simulated values of river flow in flood models is essential. The analysis regarding the calculated flow in the river brings us back to the earlier point we discussed, which is the transfer of momentum in the coupled model. As observed in our results, the coupled model tends to overestimate the river discharge, and this is attributed to the fact that in our model, this momentum is not transferred to the floodplain and does not dissipate when encountering bends. In the previous discussion, we questioned the usefulness of this feature. However, upon examining the data in our model and considering the significance of river discharge, the correct transfer of momentum regains importance and relevance.

We do not observe a time computation improvement, but this is due to the modeling of the domain, where the proportion occupied by the floodplain is much larger than the river. In the literature, tests conducted in real-world scenarios typically feature a more balanced river/floodplain size ratio, leading to significant time savings (see [12], [15], [14]). In a more realistic scenario, there is little doubt that our model would be significantly faster compared to the reference 2D model (using the same explicit 2D scheme).

Chapter 6

Conclusion

The impact of flooding is on the rise, and there is a critical need to adapt our lands. Reducing peak flow is key to mitigating the impact of a flood, and the solution proposed by the JRC in the European Union is the construction of retention areas specifically designed to decrease this maximum flow. In light of this, studying flood dynamics becomes essential. While yielding equally accurate results, the coupling methods of a 1D river with a 2D floodplain offer faster time computation compared to full 2D models, becoming a prominent means of simulating floods. There is a wide range of existing methods, with the distinction that some methods preserve momentum while others do not.

In this thesis, we have presented a discontinuous Galerkin explicit method to couple a 1D river with a 2D floodplain. The interaction between the models is achieved through the conservation of mass only, using the weir equation. The weir equation provides the flow rate of water between two domains, as a function of the water height above a structure separating two domains. This approach considers the presence of levees between rivers and floodplains, which are formed by sediments deposited during flooding events. The exchange of information occurs laterally, meaning that the 1D river is bordered by elements of the floodplain, establishing a better configuration than a frontal connection to minimize momentum transfer. The model also requires conditions to activate or deactivate the coupling system based on water levels on both sides of the wall. An algorithm for wetting and drying, which allows for the drying of 2D nodes without producing non-physical results, has also been implemented.

During our initial tests, we verified the mass conservation and stability of our model using a simple test case. We then identified the configuration of a reference 2D model that yielded the most similar results, which involved a straight river surrounded by a thin wall. This wall reduces the transfer of momentum between the

floodplain and the river, bringing it closer to our model. This optimal configuration allowed us to closely match the models in terms of mass evolution in the floodplain and the river.

We then used this ideal configuration in a more realistic case, incorporating bottom friction, the Wetting and Drying Algorithm, and basin emptying to simulate a river overflowing into a floodplain. The results showed again a significant similarity between the models in terms of mass and potential energy evolution in both the river and the floodplain. However, a slight discrepancy was observed in the evolution of kinetic energy, leading to a discussion about the impact of momentum conservation in coupled schemes for river flood analysis. In a case where the river surface area is equivalent to that of the floodplain, the simulation time is nearly halved when using the coupled model.

The bathymetry used in the final test is more realistic and deviates from the idealized model presented before. By not incorporating walls in the reference model and introducing a bifurcation, the transfer of momentum becomes more significant, and a clear disparity between the two models in terms of floodplain mass is observed. But we can evaluate the usefulness of this model by examining another variable, the river discharge. In a risk assessment scenario, the study of the peak flow is crucial, and the results of both models fit quite well, demonstrating potential in flood studies.

6.1 Shortcomings and future work

The model still faces certain challenges.

First, the equation used in the model has its own weaknesses. The lack of momentum transfer in the model is the most obvious, and addressing this would require a revision of the model. However, a middle ground could be considered. As we have seen, the weir equation is based on several assumptions, including the approximation of the total energy head (H_1) by the height above the weir (h_1). This assumption works quite well in the case of lateral coupling. Since the momentum in a straight river is mainly unidirectional, there is minimal lateral momentum transfer. However, when the river has bends and is no longer truly unidirectional, the effects of transmitted momentum become more significant. For future work, we have observed that the equation of the weir suggests a velocity coefficient, denoted as $C_v = (\frac{H_1}{h_1})^{1.5}$, which takes into account the total energy head

level (H_1) and could potentially enhance the model's effectiveness.

Secondly, the coupling equation does not consider the smaller water level between the two sides of the structure, it only depends on the highest level. To address this issue, an alternative formula (Eq. 3.20) has been implemented, but it has not been further discussed. In future work, evaluating this alternative equation in comparison to the one used in this thesis could be done using a laboratory test case, thereby addressing these limitations. For example, Morales-Hernandez et al. [20] conducted a laboratory test on a channel representing the floodplain, equipped with gauge points to measure water levels at specific locations (Fig. 6.1). The

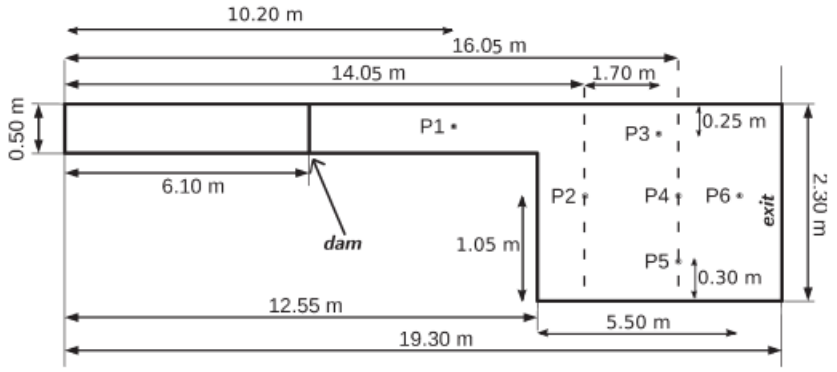

Figure 6.1: Laboratory test case in [20] with geometrical data and position of the gauge points.

reservoir at the upstream end of the channel experienced a dam break, resulting in flow propagation toward the gauge stations. This configuration can be replicated using SLIM, and if any necessary information is missing for the coupled model setup, alternative methods can be employed to validate the model data against laboratory cases.

The model is explicit, which means that the time step is limited, and in our case, it will be kept at $\Delta t = 0.001$s. We have identified that our model is faster than the full 2D reference model, which uses the same explicit scheme. The computation time has not been compared to an implicit reference model, which would use a larger time step and therefore be faster overall. One potential improvement is to adapt the model to an implicit formulation, allowing for an increased time step and thus shorter simulation time.

The full 2D reference model also incorporates simplifications, and while it is more accurate than our coupled model, it does not precisely represent real-world

phenomena. As discussed in the introduction, other coupling methods typically compare their results with satellite images of river floods or gauge station measurements. Therefore, a promising avenue would be to analyze our model using field data, from real flood events by example. SLIM has been successfully applied to numerous real-world cases, and this thesis can pave the way for simulating river floods occurring in different parts of the world.

Based on realistic and relevant assumptions, the model has demonstrated satisfactory results in terms of mass transfer and the evaluation of river discharge. Under appropriate conditions, it offers time savings compared to full 2D simulations using the same scheme. Although further comprehensive testing and improvements are still required, the model shows significant potential in the study of river floods.

Appendix A

Additional Wetting and Drying process in SLIM2D

This appendix presents an additional feature of the Wetting and Drying Algorithm present in SLIM2D, but not utilized in this thesis. When a node runs dry, the flow direction is determined by the surface elevation gradient between each node.

- If the flow leaves the empty node, we must disregard the gravitational force acting on it so as not to remove material from an already empty element.
- If the flow moves from higher-elevation nodes to the dry node, we should keep the gravity term since the dry element should fill up.

In order to meet these conditions in the algorithm, we introduce a variable s for each element :

$$s = max(\eta) + min(h) \tag{A.1}$$

with maximum surface elevation (η) and the minimum bathymetry (h) on the element. We define an threshold value ξ such that :

- If $s < \xi$, the gravity term is canceled to ensure a positive mean water depth H over each element at the end of each time step.
- If $s > \xi$, we cannot simply switch on the gravity term, because otherwise the algorithm would not be usable in an implicit temporal scheme. We have to regularize this value, this is done by multiplying the gravitational fluxes by a blending parameter alpha :

$$\alpha = \min(1, \max(0, \frac{s - \xi}{4\xi})) \tag{A.2}$$

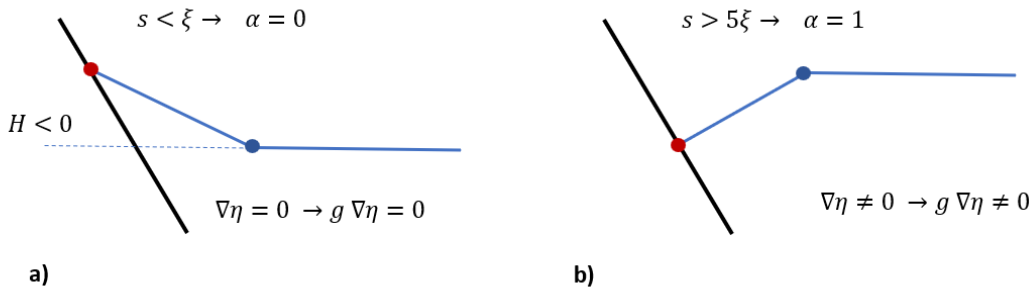

Figure A.1: Evolution of free surface in the wetting and drying algorithm. Bottom (black line), water surface (blue line), water surface in dry cell (dashed line) and cell nodes (dots), [21].

Thus when s is included between ξ and 5ξ, the value of α is interpolated from 0 to 1. Indeed, if the value of s is less than ξ, the parameter α is 0 and the gravity term is canceled. Then if s is bigger than ξ, the value of α converges rapidly to 1. In addition, we restrict the water depth to the value η in the bottom drag and wind stress parameterization, and apply a slope-limiting algorithm on each element to guarantee a positive depth at the nodes.
A theoretical and real domain test case shows that this algorithm reproduces well the process of watering and dewatering, as shown in [21].

Appendix B

Additional plot of mass conservation assessment

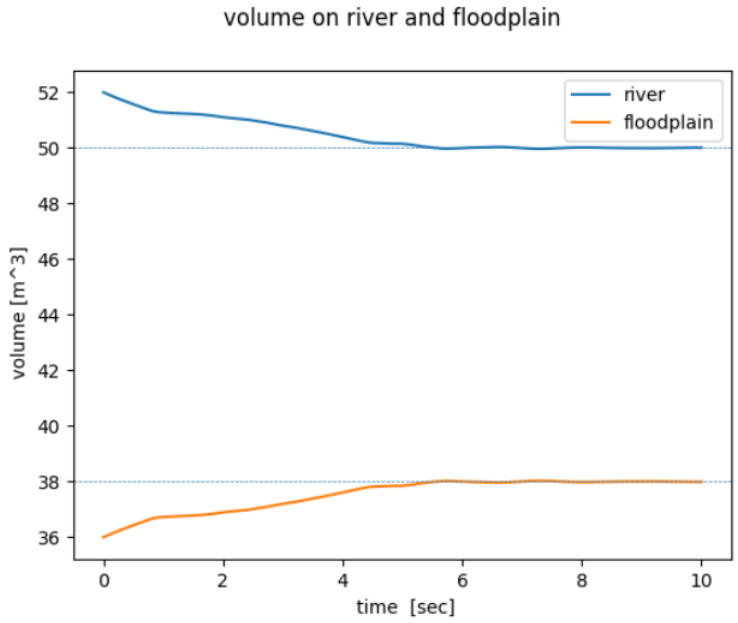

Figure B.1: Plot of the volume on the river and floodplain in the mass conservation assessment using submerged flow equations

By using the modified source term equations, a noticeable change in the pattern of mass evolution is observed. Instead of reaching equilibrium around 3 seconds, equilibrium is reached around 5 seconds after the simulation starts. This significant change raises the question of which model of source term most closely resembles reality.

Appendix C

Manning roughness coefficient for floodplains and channels

This appendix contains the values of adjustment coefficients used to evaluate Manning's coefficient in both the river and floodplain (in [16]).

Flood-plain conditions		*n* value adjustment	Example
Degree of irregularity (n_1)	Smooth	0.000	Compares to the smoothest, flattest flood plain attainable in a given bed material.
	Minor	0.001–0.005	Is a flood plain slightly irregular in shape. A few rises and dips or sloughs may be visible on the flood plain.
	Moderate	0.006–0.010	Has more rises and dips. Sloughs and hummocks may occur.
	Severe	0.011–0.020	Flood plain very irregular in shape. Many rises and dips or sloughs are visible. Irregular ground surfaces in pastureland and furrows perpendicular to the flow are also included.
Variation of flood-plain cross section (n_2)		0.0	Not applicable.
Effect of obstructions (n_3)	Negligible	0.000–0.004	Few scattered obstructions, which include debris deposits, stumps, exposed roots, logs, or isolated boulders, occupy less than 5 percent of the cross-sectional area.
	Minor	0.005–0.019	Obstructions occupy less than 15 percent of the cross-sectional area.
	Appreciable	0.020–0.030	Obstructions occupy from 15 to 50 percent of the cross-sectional area.
Amount of vegetation (n_4)	Small	0.001–0.010	Dense growth of flexible turf grass, such as Bermuda, or weeds growing where the average depth of flow is at least two times the height of the vegetation, or supple tree seedlings such as willow, cottonwood, arrowweed, or saltcedar growing where the average depth of flow is at least three times the height of the vegetation.
	Medium	0.011–0.025	Turf grass growing where the average depth of flow is from one to two times the height of the vegetation, or moderately dense stemmy grass, weeds, or tree seedlings growing where the average depth of flow is from two to three times the height of the vegetation; brushy, moderately dense vegetation, similar to 1- to 2-year-old willow trees in the dormant season.
	Large	0.025–0.050	Turf grass growing where the average depth of flow is about equal to the height of the vegetation, or 8- to 10-year-old willow or cottonwood trees intergrown with some weeds and brush (none of the vegetation in foliage) where the hydraulic radius exceeds 2 ft, or mature row crops such as small vegetables, or mature field crops where depth of flow is at least twice the height of the vegetation.
	Very large	0.050–0.100	Turf grass growing where the average depth of flow is less than half the height of the vegetation, or moderate to dense brush, or heavy stand of timber with few down trees and little undergrowth where depth of flow is below branches, or mature field crops where depth of flow is less than the height of the vegetation.
	Extreme	0.100–0.200	Dense bushy willow, mesquite, and saltcedar (all vegetation in full foliage), or heavy stand of timber, few down trees, depth of flow reaching branches.
Degree of meander (m)		1.0	Not applicable.

Figure C.1: Adjustment values for factors that affect manning roughness coefficient for floodplains, in [16].

Channel conditions		n value adjustment[1]	Example
Degree of irregularity (n_1)	Smooth	0.000	Compares to the smoothest channel attainable in a given bed material.
	Minor	0.001–0.005	Compares to carefully dredged channels in good condition but having slightly eroded or scoured side slopes.
	Moderate	0.006–0.010	Compares to dredged channels having moderate to considerable bed roughness and moderately sloughed or eroded side slopes.
	Severe	0.011–0.020	Badly sloughed or scalloped banks of natural streams; badly eroded or sloughed sides of canals or drainage channels; unshaped, jagged, and irregular surfaces of channels in rock.
Variation in channel cross section (n_2)	Gradual	0.000	Size and shape of channel cross sections change gradually.
	Alternating occasionally	0.001–0.005	Large and small cross sections alternate occasionally, or the main flow occasionally shifts from side to side owing to changes in cross-sectional shape.
	Alternating frequently	0.010–0.015	Large and small cross sections alternate frequently, or the main flow frequently shifts from side to side owing to changes in cross-sectional shape.
Effect of obstruction (n_3)	Negligible	0.000–0.004	A few scattered obstructions, which include debris deposits, stumps, exposed roots, logs, piers, or isolated boulders, that occupy less than 5 percent of the cross-sectional area.
	Minor	0.005–0.015	Obstructions occupy less than 15 percent of the cross-sectional area, and the spacing between obstructions is such that the sphere of influence around one obstruction does not extend to the sphere of influence around another obstruction. Smaller adjustments are used for curved smooth-surfaced objects than are used for sharp-edged angular objects.
	Appreciable	0.020–0.030	Obstructions occupy from 15 to 50 percent of the cross-sectional area, or the space between obstructions is small enough to cause the effects of several obstructions to be additive, thereby blocking an equivalent part of a cross section.
	Severe	0.040–0.050	Obstructions occupy more than 50 percent of the cross-sectional area, or the space between obstructions is small enough to cause turbulence across most of the cross section.
Amount of vegetation (n_4)	Small	0.002–0.010	Dense growths of flexible turf grass, such as Bermuda, or weeds growing where the average depth of flow is at least two times the height of the vegetation; supple tree seedlings such as willow, cottonwood, arrowweed, or saltcedar growing where the average depth of flow is at least three times the height of the vegetation.
	Medium	0.010–0.025	Turf grass growing where the average depth of flow is from one to two times the height of the vegetation; moderately dense stemmy grass, weeds, or tree seedlings growing where the average depth of flow is from two to three times the height of the vegetation; brushy, moderately dense vegetation, similar to 1- to 2-year-old willow trees in the dormant season, growing along the banks, and no significant vegetation is evident along the channel bottoms where the hydraulic radius exceeds 2 ft.
	Large	0.025–0.050	Turf grass growing where the average depth of flow is about equal to the height of the vegetation; 8- to 10-year-old willow or cottonwood trees intergrown with some weeds and brush (none of the vegetation in foliage) where the hydraulic radius exceeds 2 ft; bushy willows about 1 year old intergrown with some weeds along side slopes (all vegetation in full foliage), and no significant vegetation exists along channel bottoms where the hydraulic radius is greater than 2 ft.
	Very large	0.050–0.100	Turf grass growing where the average depth of flow is less than half the height of the vegetation; bushy willow trees about 1 year old intergrown with weeds along side slopes (all vegetation in full foliage), or dense cattails growing along channel bottom; trees intergrown with weeds and brush (all vegetation in full foliage).
Degree of meandering[2] (m)	Minor	1.00	Ratio of the channel length to valley length is 1.0 to 1.2.
	Appreciable	1.15	Ratio of the channel length to valley length is 1.2 to 1.5.
	Severe	1.30	Ratio of the channel length to valley length is greater than 1.5.

[1] Adjustments for degree of irregularity, variations in cross section, effect of obstructions, and vegetation are added to the base n value (table 1) before multiplying by the adjustment for meander.

[2] Adjustment values apply to flow confined in the channel and do not apply where downvalley flow crosses meanders.

Figure C.2: Adjustment values for factors that affect manning roughness coefficient for channels, in [16].

Bibliography

[1] R Wallemacq P. & House. "Economic Losses, Poverty & DISASTERS 1998-2017". In: *CRED and UNISDR* (2018).

[2] European Commission. Joint Research Centre. *Adapting to rising river flood risk in the EU under climate change: JRC PESETA IV project: Task 5.* Publications Office, 2020. DOI: 10.2760/14505. URL: https://data.europa.eu/doi/10.2760/14505.

[3] Francis W. Zwiers & Gabriele C. Hegerl Seung-Ki Min Xuebin Zhang. "Human contribution to more-intense precipitation extremes". In: *Nature* 470 (2011), pp. 378–341.

[4] Yukiko Imada & Hideo Shiogama HairetiAlifu Yukiko Hirabayashi. "Enhancement of river fooding due to global warming". In: *Scientifc Reports* 20687 (2022).

[5] Jafar Yavarian, Nazanin Z Shafiei-Jandaghi, and Talat Mokhtari-Azad. "Possible viral infections in flood disasters: review considering 2019 spring floods in Iran". In: *Iranian Journal of Microbiology* 11.2 (2019), pp. 85–89.

[6] Francesco Dottori, Lorenzo Mentaschi, Alessandra Bianchi, Lorenzo Alfieri, and Luc Feyen. "Cost-effective adaptation strategies to rising river flood risk in Europe". In: *Nature Climate Change* 13.2 (2023), pp. 196–202. DOI: 10.1038/s41558-022-01540-0. URL: https://doi.org/10.1038/s41558-022-01540-0.

[7] Kris A. Johnson, Oliver E. J. Wing, Paul D. Bates, Joseph Fargione, Timm Kroeger, et al. "A benefit–cost analysis of floodplain land acquisition for US flood damage reduction". In: *Nature Sustainability* 3.1 (2019), pp. 56–62. DOI: 10.1038/s41893-019-0437-5. URL: https://doi.org/10.1038/s41893-019-0437-5.

[8] Till Branß, Francisco Núñez-González, and Jochen Aberle. "Fluvial levees in compound channels: a review on formation processes and the impact of bedforms and vegetation". In: *Environmental Fluid Mechanics* 22.2-3

(2022), pp. 559–585. DOI: 10.1007/s10652-022-09850-9. URL: https://doi.org/10.1007/s10652-022-09850-9.

[9] J. Teng, A.J. Jakeman, J. Vaze, B.F.W. Croke, D. Dutta, et al. "Flood inundation modelling: A review of methods, recent advances and uncertainty analysis". In: *Environmental Modelling Software* 90 (2017), pp. 201–216. ISSN: 1364-8152. DOI: https://doi.org/10.1016/j.envsoft.2017.01.006. URL: https://www.sciencedirect.com/science/article/pii/S1364815216310040.

[10] Dale R. Durran. *Numerical Methods for Fluid Dynamics With Applications to Geophysics*. second. Vol. texts in applied mathematics. Springer, 2010.

[11] Weiming Wu; Wolfgang Rodi; Thomas Wenka. "3D Numerical Modeling of Flow and Sediment Transport in Open Channels". In: *Journal of Hydraulic Engineering* (2000).

[12] M. Morales-Hernández, G. Petaccia, P. Brufau, and P. Garcı´a-Navarro. "Conservative 1D–2D coupled numerical strategies applied to river flooding: The Tiber (Rome)". In: *Applied Mathematical Modelling* 40.3 (2016), pp. 2087–2105. DOI: 10.1016/j.apm.2015.08.016. URL: https://doi.org/10.1016/j.apm.2015.08.016.

[13] E D Fernández-Nieto, J Marin, and J Monnier. "Coupling superposed 1D and 2D shallow-water models: Source terms in finite volume schemes". en. In: *Comput. Fluids* 39.6 (2010), pp. 1070–1082.

[14] Soumendra Nath Kuiry, Dhrubajyoti Sen, and Paul D. Bates. "Coupled 1D–Quasi-2D Flood Inundation Model with Unstructured Grids". In: *Journal of Hydraulic Engineering* 136.8 (2010), pp. 493–506. DOI: 10.1061/(asce)hy.1943-7900.0000211. URL: https://doi.org/10.1061/(asce)hy.1943-7900.0000211.

[15] E. Bladé, M. Gómez-Valentín, J. Dolz, J.L. Aragón-Hernández, G. Corestein, et al. "Integration of 1D and 2D finite volume schemes for computations of water flow in natural channels". In: *Advances in Water Resources* 42 (2012), pp. 17–29. ISSN: 0309-1708. DOI: https://doi.org/10.1016/j.advwatres.2012.03.021. URL: https://www.sciencedirect.com/science/article/pii/S0309170812000760.

[16] Verne R. Schneider Georges J. Arcement JR. "Guide for Selecting Manning's Roughness Coefficients for Natural Channels and Flood Plains". In: *United States Geological Survey Water-Supply* (1989).

[17] M.G. Bos. *Discharge measurement structures*. International Institute for Land Reclamation and improvement, Wageningen, The Netherlands., 1976.

[18] Pascal Finaud-Guyot, Carole Delenne, Vincent Guinot, and Cécile Llovel. "1D–2D coupling for river flow modeling". In: *Comptes Rendus Mécanique* 339.4 (2011), pp. 226–234. ISSN: 1631-0721. DOI: https://doi.org/10.1016/j.crme.2011.02.001. URL: https://www.sciencedirect.com/science/article/pii/S163107211100026X.

[19] Fang Zhao, Ted I E Veldkamp, Katja Frieler, Jacob Schewe, Sebastian Ostberg, et al. "The critical role of the routing scheme in simulating peak river discharge in global hydrological models". In: *Environmental Research Letters* 12.7 (June 2017), p. 075003. DOI: 10.1088/1748-9326/aa7250. URL: https://doi.org/10.1088/1748-9326/aa7250.

[20] M. Morales-Hernández, P. Garcı´a-Navarro, J. Burguete, and P. Brufau. "A conservative strategy to couple 1D and 2D models for shallow water flow simulation". In: *Computers &amp Fluids* 81 (July 2013), pp. 26–44. DOI: 10.1016/j.compfluid.2013.04.001. URL: https://doi.org/10.1016/j.compfluid.2013.04.001.

[21] HA Le, J Lambrechts, S Ortleb, et al. "An implicit wetting–drying algorithm for the discontinuous Galerkin method: Application to the Tonle Sap, Mekong River Basin". In: *Environmental Fluid Mechanics* 20.4 (2020), pp. 923–951. DOI: 10.1007/s10652-019-09732-7.

UNIVERSITÉ CATHOLIQUE DE LOUVAIN
École polytechnique de Louvain
Rue Archimède, 1 bte L6.11.01, 1348 Louvain-la-Neuve, Belgique | **www.uclouvain.be/epl**